Published in final edited form as:

Cell. 2022 August 18; 185(17): 3232–3247.e18. doi:10.1016/j.cell.2022.06.048.

Epigenetic reader SP140 loss of function drives Crohn's disease due to uncontrolled macrophage topoisomerases

Hajera Amatullah[1,2,7], **Isabella Fraschilla**[1,2,3], **Sreehaas Digumarthi**[1], **Julie Huang**[1], **Fatemeh Adiliaghdam**[1,2], **Gracia Bonilla**[4], **Lai Ping Wong**[4], **Marie-Eve Rivard**[5], **Claudine Beauchamp**[5], **Virginie Mercier**[5], **Philippe Goyette**[5], **Ruslan I. Sadreyev**[4], **Robert M. Anthony**[6], **John Rioux**[5], **Kate L. Jeffrey**[1,2,3,7,8,*]

[1]Center for the Study of Inflammatory Bowel Disease, Division of Gastroenterology, Department of Medicine, Massachusetts General Hospital Research Institute, Boston, MA 02114, USA

[2]Harvard Medical School, Boston, MA 02115, USA

[3]Program in Immunology, Harvard Medical School, Boston, MA 02115, USA

[4]Department of Molecular Biology, Department of Pathology, Massachusetts General Hospital, Harvard Medical School, Boston, MA 02114, USA

[5]Montreal Heart Institute, Montreal, QC H1T 1C8, Canada

[6]Center for Immunology and Inflammatory Diseases, Division of Rheumatology, Allergy and Immunology, Department of Medicine, Massachusetts General Hospital, Harvard Medical School, Boston, MA, USA

[7]Present address: Moderna Inc., 200 Technology Square, Cambridge, MA 02138, USA

[8]Lead contact

SUMMARY

[*]Correspondence: kjeffrey@mgh.harvard.edu.

AUTHOR CONTRIBUTIONS

H.A. contributed most experiments including proteomic analysis, coIP experiments, mouse experiments, TOP functional assays, ChIP, multiplexed indexed chromatin immunoprecipitation (MintChIP) and CUT&Tag experiments, developed methods, and generated resources. I.F. generated SP140 mutants and contributed experiments. S.D. contributed coIP experiments, CRISPR-Cas9 mouse macrophages, primary human macrophage experiments, and RNA-seq library preparation. J.H. conducted qPCRs of double KDs and with F.A. contributed to endpoint measurements of mouse experiments. G.B., L.P.W., and R.I.S. contributed RNA-seq analysis, CUT&Tag analysis, MintChIP analysis, and ChIP correlations. R.M.A. supervised some *in vivo* experiments and provided reagents; and M.R., C.B., V.M., P.G., and J.R. generated iPSC-derived CD human macrophages from $SP140^{mut}$ CD patients. K.L.J. conceived and supervised the study, obtained funding, and wrote the final manuscript along with H.A.

SUPPLEMENTAL INFORMATION

Supplemental information can be found online at https://doi.org/10.1016/j.cell.2022.06.048.

DECLARATION OF INTERESTS

K.L.J. and H.A. are employees and shareholders of Moderna Inc., 200 Technology Square, Cambridge, MA 02138, since November 2021 and May 2022, respectively, after the time that this research was conducted. K.L.J. is a member of the scientific advisory board for Ancilia Biosciences. None of these relationships influenced the work in this study.

INCLUSION AND DIVERSITY

We worked to ensure gender balance in the recruitment of human subjects. We worked to ensure ethnic or other types of diversity in the recruitment of human subjects. We worked to ensure that the study questionnaires were prepared in an inclusive way. We worked to ensure sex balance in the selection of non-human subjects. We worked to ensure diversity in experimental samples through the selection of the cell lines. One or more of the authors of this paper self-identifies as an underrepresented ethnic minority in science. The author list of this paper includes contributors from the location where the research was conducted who participated in the data collection, design, analysis, and/or interpretation of the work.

How mis-regulated chromatin directly impacts human immune disorders is poorly understood. Speckled Protein 140 (SP140) is an immune-restricted PHD and bromodomain-containing epigenetic ‘‘reader,’’ and SP140 loss-of-function mutations associate with Crohn’s disease (CD), multiple sclerosis (MS), and chronic lymphocytic leukemia (CLL). However, the relevance of these mutations and mechanisms underlying SP140-driven pathogenicity remains unexplored. Using a global proteomic strategy, we identified SP140 as a repressor of topoisomerases (TOPs) that maintains heterochromatin and macrophage fate. In humans and mice, SP140 loss resulted in unleashed TOP activity, de-repression of developmentally silenced genes, and ultimately defective microbe-inducible macrophage transcriptional programs and bacterial killing that drive intestinal pathology. Pharmacological inhibition of TOP1/2 rescued these defects. Furthermore, exacerbated colitis was restored with TOP1/2 inhibitors in Sp140$^{-/-}$ mice, but not wild-type mice, *in vivo*. Collectively, we identify SP140 as a TOP repressor and reveal repurposing of TOP inhibition to reverse immune diseases driven by SP140 loss.

Graphical abstract

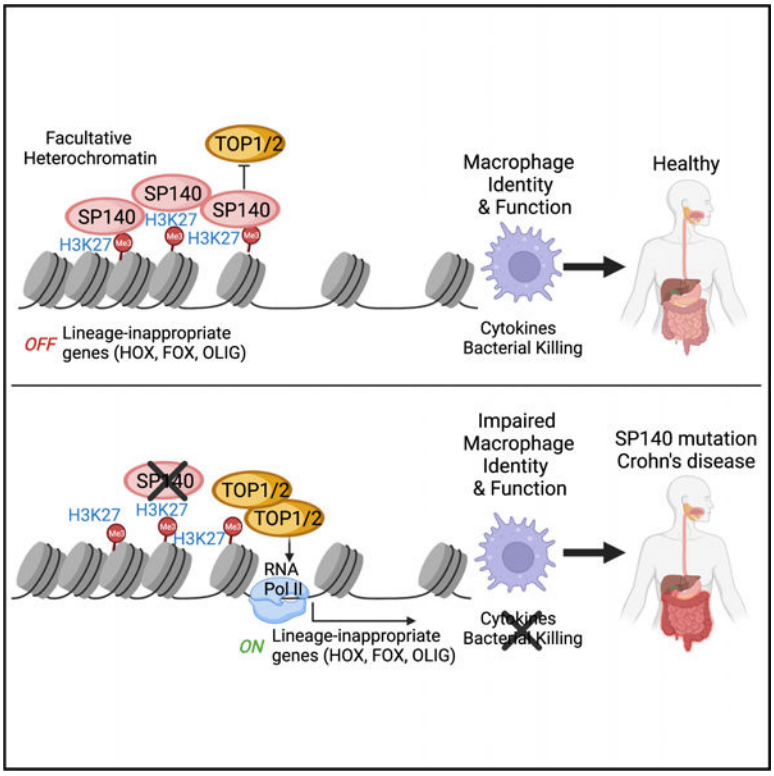

In brief

SP140 acts as a repressor of topoisomerases and maintains macrophage cytokine and bacterial killing functions, preventing inflammatory conditions such as Crohn’s disease.

INTRODUCTION

Chromatin regulatory proteins are indispensable for both maintenance of immune cell identity and integration of environmental cues. In particular, recognition of dynamic posttranslational modifications on histones by chromatin ‘‘readers’’ is a critical step in this process (Smale et al., 2014; Soshnev et al., 2016; Wan et al., 2020; Wen et al., 2014). Dysregulated chromatin readers and aberrant chromatin architecture are central events in cancer (Filippakopoulos et al., 2010; Wan et al., 2020; Wen et al., 2014); therefore, targeting such pathways holds clinical promise (Dawson et al., 2011; Filippakopoulos et al., 2010; Nicodeme et al., 2010). However, little is known about how altered chromatin readers may directly contribute to and facilitate tailored therapies for human immune diseases.

The complex immune disorders Crohn’s disease (CD), multiple sclerosis (MS), and chronic lymphocytic leukemia (CLL) result from both genetic susceptibility and environmental cues and, despite their clinical heterogeneity, share many identified genetic risk variants, suggesting common pathogenic mechanisms (Cotsapas and Hafler, 2013; Franke et al., 2010; International Multiple Sclerosis Genetics et al., 2013; Jostins et al., 2012; Sillé et al., 2012). Mutations within epigenetic reader, Speckled Protein 140 (SP140), is one such common genetic risk factor for these three immune diseases (Fraschilla and Jeffrey, 2020; International Multiple Sclerosis Genetics et al., 2013; Jostins et al., 2012; Sillé et al., 2012). SP140 belongs to the SP family consisting of SP100, SP110, and SP140L, which have high homology with autoimmune regulator (AIRE) (Fraschilla and Jeffrey, 2020; Gibson et al., 1998). SPs all contain an N-terminal caspase activation recruitment domain (CARD) domain, an intrinsically disordered region (IDR) and multiple ‘‘reader’’ modules including a SAND domain, a plant homeobox domain (PHD), and a bromodomain (BRD) (Fraschilla and Jeffrey, 2020; Figure 1A), indicative of a role in chromatin regulation. Moreover, SP family members are components of promyelocytic leukemia nuclear bodies (PML-NBs), which are ill-defined subnuclear structures regulated by a variety of cellular stresses such as virus infection, interferon (IFN), and DNA damage, with implicated roles in many cellular processes, including gene repression and higher order chromatin organization (Huoh et al., 2020; Lallemand-Breitenbach and de Thé , 2010).

Of the SPs, SP140 expression is uniquely restricted to immune cells (Bloch et al., 1996), with highest levels in activated macrophages and mature B cells (Mehta et al., 2017). Initial studies found SP140 to be critical for appropriate macrophage cytokine responses to bacteria or virus (Ji et al., 2021; Karaky et al., 2018; Mehta et al., 2017). Moreover, we recently demonstrated that SP140 acts as a co-repressor of lineage-inappropriate genes such as *HOX* in mature human macrophages, preferentially occupying promoters of these silenced genes within facultative heterochromatin regions marked by H3K27me3 to maintain macrophage identity and functional responses (Mehta et al., 2017). The CD-, MS-, and CLL-associated genetic variants of SP140 alter SP140 mRNA splicing and diminish SP140 protein (Matesanz et al., 2015; Mehta et al., 2017). Therefore, we asked mechanistically how this immune chromatin reader normally acts and how perturbations lead to altered SP140 structure and function on chromatin and eventually immune disease, with the intent to identify therapeutic interventions.

RESULTS

Elucidation of the SP140 interactome: DNA unwinders and chromatin remodelers

To gain molecular insights into the normal function of SP140, we elucidated the SP140 interactome. We ectopically expressed FLAG-tagged human SP140 or FLAG-empty vector (FLAG-EV) in HEK293T cells (Figure S1A, related to Figure 1) and subsequently performed mass spectrometry (MS) on FLAG co-immunoprecipitants (coIPs). To efficiently discriminate confident interacting proteins from false-positive or contaminant proteins, the probability of bona fide protein-protein interactions was analyzed using the contaminant repository of affinity matrix (CRAPome) and significance analysis of interactome (SAINT) scores (Mellacheruvu et al., 2013; Figures 1A and S1B; Table S1, related to Figure 1). This approach identified the top significant interactors of SP140 to be: topoisomerases (TOP)1, TOP2A, TOP2B, DNA-dependent protein kinase (DNA-PK), facilitates chromatin transactions (FACT) subunits SUPT16H and SSRP1, as well as the ATPase subunit of the ISWI family of chromatin remodelers, switch/sucrose non-fermentable (SWI/SNF) related, matrix-associated, actin-dependent regulator of chromatin, subfamily A, member 5 (SMARCA5, Figure 1A). The top 1% of SP140 interacting partners (with false discovery rate [FDR], of less than 1%) broadly clustered under three functional groups (Szklarczyk et al., 2019): ‘‘chromatin organization and DNA unwinding,’’ ‘‘RNA processing and splicing,’’ and ‘‘metabolic processes’’ (Figure 1B). Gene ontology (GO) analyses confirmed that the SP140 interactome was associated with ‘‘DNA topological change,’’ ‘‘nucleosome organization,’’ and ‘‘DNA unwinding’’ (Figure S1C, related to Figure 1).

Topoisomerases 1 and 2 are SP140 protein partners

We previously demonstrated that SP140 represses chromatin accessibility in human macrophages (Mehta et al., 2017); hence, we explored SP140 interactions with chromatin organization and DNA unwinding proteins TOP1, TOP2A, TOP2B, DNA-PK SUPT16H, SSRP1, and SMARCA5. Through immunoprecipitation (IP) of FLAG-SP140 in HEK293T expressing FLAG-SP140 or FLAG-EV and immunoblot of FLAG, we confirmed SP140 interacted with endogenous TOP1, TOP2A, TOP2B, DNA-PK, SUPT16H, SSRP1, and SMARCA5 (Figure 1C). Reciprocal IP of endogenous TOP1, TOP2A, DNA-PK, SUPT16H, SSRP1, and SMARCA5 and immunoblot of FLAG validated these interactions (Figure S1D, related to Figure 1). Moreover, IP of endogenous SP140 in human monocyte THP1 cells and primary human peripheral blood mononuclear cells (PBMCs) confirmed these interactions exist in relevant immune cells (Figures 1D and S1E, related to Figure 1). SP140 complexes with TOP1, TOP2A, TOP2B, DNA-PK, SUPT16H, SSRP1, and SMARCA5 required structured DNA, since addition of the intercalating agent ethidium bromide (EtBr) disrupted their interactions (Figures S1F and S1G, related to Figure 1). Furthermore, the chromatin ‘‘reading’’ PHD and BRD of SP140 were also necessary for these protein-protein interactions (Figure 1E). However, the CARD domain, known for protein multimerization and localization of SP proteins to PML bodies (Huoh et al., 2020) was not required for SP140 interactions with TOPs (Figure S1H, related to Figure 1). In addition, SP140 has been previously identified to be a SUMO target (Zucchelli et al., 2019). However, mutation of the top predicted SUMOylation site within SP140 (K762A), previously shown to disrupt SP140 SUMOylation (Zucchelli et al., 2019), had no impact on SP140 interaction with

TOPs (Figure S1I, related to Figure 1). Thus, SP140 interaction with chromatin via its PHD and BRD reader domains is the primary driver of SP140-TOP complex formation. We next assessed whether TOPs or DNA-PK may be primary interacting proteins upon which the complex formed. Exposure of cells to TOP1 inhibitor Topotecan (TPT) or TOP2 inhibitor Etoposide (ETO, Figure S1J, related to Figure 1) or siRNA-mediated knockdown (KD) of *TOP1* or *TOP2A* resulted in a loss of SP140 and TOP interaction but did not affect SP140 interactions with DNA-PK, SUPT16H, or SMARCA5 (Figure S1K, related to Figure 1). Similarly, DNA-PK (*PRKDC*) siRNA led to partial loss of SP140 binding to TOP1, but all other interactions remained intact (Figure S1L, related to Figure 1). Thus, SP140 forms multiple distinct protein complexes, characteristic of flexible IDR-containing proteins that form phase-separated condensates (Sabari et al., 2018). Notably, many of the SP140 interacting proteins we identified were previously found to interact with AIRE, which shares protein homology with SP140 (Figure S2A, related to Figure 1) (Abramson et al., 2010; Bansal et al., 2017). However, although AIRE promotes transcription of peripheral-tissue antigens in medullary thymic epithelial cells (mTECs) (Mathis and Benoist, 2009), our current working model is one in which SP140 functions as a transcriptional repressor. Consistent with this notion, the common SP140 and AIRE interacting partners included chromatin remodeling and DNA unwinding proteins (TOP1, TOP2A, TOP2B, DNA-PK, and SUPT16H), whereas transcriptional elongation machineries (PTEFb and BRD4) that enable transcription were exclusively associated with AIRE and not SP140 (Figure S2B, related to Figure 1). Furthermore, although SP140 and AIRE are generally expressed in different cell types (Fraschilla and Jeffrey, 2020), we co-transfected AIRE and SP140 and found that SP140 and AIRE did not compete for binding of endogenous TOP1 or TOP2A (Figure S2C, related to Figure 1), suggesting that SP140 and AIRE interact with distinct pools of TOPs.

Loss of SP140-TOP interactions in CD patients bearing SP140 mutants

We next examined the consequence of disease risk loss-of-function SP140 on its ability to form the identified protein complexes. The genomic region containing SP140 was definitively associated with inflammatory bowel disease in one of the largest association studies that consisted of ~15k CD, 11k Ulcerative Colitis, and ~16k controls (Jostins et al., 2012). It was identified as being primarily associated with CD, with an odds ratio for CD of 1.13 (95% CI, 1.089–1.18). In European-derived populations where this variant was identified, rs28445040, which encodes the splicing variant studied herein, has a minor allele frequency of ~0.20 in patients with CD and ~0.18 in controls. This variant of SP140 is at the start of exon 7 that changes the RNA from UCCU to UCUU (Figures S3A and S3B, related to Figure 1). UCUU is a known binding site of polypyrimidine tract binding protein (PTB), an established exon repressor during mRNA splicing (Hamon et al., 2004; Xue et al., 2009). UCUU is also at the start of exon 11, possibly explaining why a significant elevation of an SP140 mRNA isoform lacking both exons 7 and 11 was observed with CD-associated SP140 mutations (Mehta et al., 2017). Beyond a splicing defect, this synonymous polymorphism may also affect the rate of protein translation and stability (Sauna and Kimchi-Sarfaty, 2011) (Figure S3B, related to Figure 1). Indeed, we confirmed that fresh PBMCs taken from CD patients homozygous for SP140 mutations had equivalent amounts of SP140 exon 1 but significantly reduced levels of exon 7 (Figure S3C,

related to Figure 1), indicative of exon 7 exclusion. Furthermore, lymphoblastoid B cell lines (LBLs) derived from CD patients bearing SP140 CD-associated mutations displayed a consistent loss of protein compared with controls (Figure S3D, related to Figure 1). We also converted these LBLs to induced pluripotent stem cells (iPSCs) and differentiated the iPSCs into human M(IFNg) macrophages to reveal that the diminished SP140 protein was apparent in SP140^{mut} macrophages (Figure S3E, related to Figure 1). We next examined the dominant interactors of endogenous SP140 in patient-derived LBLs by MS and found that similar to observations in HEK293T and THP1 cells, the top SP140 interactors were chromatin remodeling and DNA unwinding proteins TOP1, TOP2A, TOP2B, DNA-PK, SUPT16H, and SSRP1, which was confirmed by coIP (Figures 1F and 1G). Importantly, these interactions were lost in patients homozygous for loss-of-function CD-associated genetic variants of SP140 (SP140^{mut}, Figures 1F and 1G) that exhibited loss of SP140 protein. To confirm whether the loss of SP140 protein complexes was due to the total loss of SP140 or was specifically due to changes in the IDR where the excluded exons 7 and 11 normally code (Figure S3B), we constructed mutants of SP140 that lack exon 7, exon 11, or both exons 7 and 11, as observed in patients homozygous for SP140 single nucleotide polymorphism (SNP) rs28445040 (Mehta et al., 2017), as well as a mutant of SP140 lacking the entire IDR. We found that none of these locations of SP140 were required for SP140-TOP interactions, demonstrating that the loss of SP140-TOP interactions in CD patients bearing SP140 mutations is due to the total loss of SP140 protein rather than the remaining truncated SP140 lacking parts of the IDR (Figure S3F, related to Figure 1). Notably, there was not simply a loss of all SP140 interacting proteins in SP140^{mut} immune cells, but a re-wiring of the SP140 proteome was also observed. This included enhanced interactions between the remaining SP140 and proteins-associated RNA processing and splicing factors (Figures S3G and S3H, related to Figure 1) possibly skewing SP140 toward these functions. Together, these data reveal that SP140 interacts with essential DNA unwinding and chromatin remodeling proteins, and these complexes are disrupted with CD, MS, or CLL-risk SP140 loss of function.

SP140 is a negative regulator of TOP 1 and 2

The TOP enzymes TOP1 and TOP2A/B cleave one or both DNA strands, respectively, to resolve DNA topological constraints for replication, transcription, and chromatin organization (Pommier et al., 2016). For transcription, TOPs are required for the relief of torsional strain as a result of chromatin remodeling, nucleosome depletion at enhancers or promoters, as well as RNA polymerase II (RNA Pol II) pausing and elongation (Pommier et al., 2016). Furthermore, in addition to RNA Pol II itself (Baranello et al., 2016), multiple chromatin regulators and remodelers alter TOP by promoting or shielding TOP1 or 2 activity and binding (Abramson et al., 2010; Baranello et al., 2016; Dykhuizen et al., 2013; Husain et al., 2016). SP140 predominantly occupies facultative heterochromatin (Mehta et al., 2017); hence, we postulated that SP140 negatively regulates TOPs to prevent unsolicited transcription or chromatin decompaction at dynamic silent regions. Intriguingly, purified recombinant SP140 protein suppressed the ability of recombinant TOP1 to nick and unwind a supercoiled DNA substrate *in vitro* (Figure 2A). Furthermore, recombinant SP140 significantly decreased TOP2A decatenatory activity in a dose-dependent manner (Figure 2B). Upon SP140 depletion in THP1 monocytes (Figure 2C) or primary human peripheral

blood-derived macrophages (Figure 2E), we observed significantly increased TOP1 activity in nuclear lysates, both at baseline and upon lipopolysaccharide (LPS) stimulation despite unchanged TOP1 protein levels (Figures 2D and 2F). Furthermore, comparative analysis of the different SP family members (SP100, SP110, SP140, and SP140L) in human monocytes revealed that TOP repression is unique to SP140 and its paralog, SP140L (Figure S4, related to Figure 2). Conversely, overexpression of SP140 in HEK293T cells suppressed nuclear TOP1 activity in a dose-dependent manner to levels of repression observed by TPT, an FDA-approved TOP1 inhibitor that intercalates between cleaved DNA ends in the active site of the enzyme (Vos et al., 2011; Figures 2G and 2H). Importantly, immune cells bearing loss-of-function SP140 displayed significantly increased TOP1 activity that could be reversed with TPT administration (Figures 2I and 2J). Thus, our results identified SP140 as a suppressor of TOP1 and TOP2 activity and unmask a specific compromise in this hallmark function of SP140 in patients bearing CD-, MS-, and CLL-associated genetic variants of SP140.

Loss of SP140 in macrophages increases heterochromatin DNA breaks

Recruitment of TOP1 and TOP2 at gene regulatory elements leads to transcriptional-associated DNA breaks that activates DNA damage response pathways (Puc et al., 2017). Certainly, TOP-mediated double-stranded breaks (DSBs) are required for transcription initiation and elongation (Bunch et al., 2015; Ju et al., 2006). We therefore assessed levels of phosphorylation of the Serine 139 residue of the histone variant H2AX (gamma-H2AX, γH2AX), as a specific and sensitive molecular marker of DSBs and transcriptional activation. CRISPR-mediated deletion of Sp140 in Cas9 transgenic mouse macrophages or siRNA-mediated KD of SP140 in THP1 human monocytes resulted in significantly higher levels of γH2AX (Figures 3A and 3B). The enhanced γH2AX observed in SP140 KD cells was not due to differences in DNA DSBs from canonical DNA damage as cell viability, cell cycle phases, and levels of phosphorylated check-point kinase 2 (CHK2) were unaffected by SP140 depletion (Figure S5, related to Figure 3), consistent with previous findings (Kim et al., 2019). Moreover, patient-derived LBLs bearing disease-associated SP140 loss-of-function variants displayed significantly increased γH2AX, which was concomitant with the amount of SP140 protein loss (Figure 3C). We next asked if gained γH2AX in the absence of SP140 was preferentially occurring at facultative heterochromatin marked by H3K27me3, where SP140 chiefly resides (Mehta et al., 2017). Indeed, confocal microscopy of murine or human macrophages revealed that elevated γH2AX mostly occurred at the nuclear periphery upon SP140 deletion or KD (Figures 3D and 3E), where compacted H3K27me3+ facultative heterochromatin and low transcription activity is located (Buchwalter et al., 2019). Moreover, chromatin IP (ChIP) of γH2AX in primary human macrophages found a preferential gain of γH2AX at normally silenced loci *HOXA7*, HOXB9, and *FOXB1*, with unaltered γH2AX occupancy at the constitutively transcribed housekeeping gene, β-actin (*ACTB*) following siRNA-mediated KD of SP140 (Figure 3F). Thus, in the absence of SP140, transcriptional breaks and genome instability occur at normally silenced regions. To assess if levels of H3K27me3 influenced SP140 and TOP interactions, we treated macrophages with GSK343, an inhibitor of the H3K27me3 ‘‘writer’’ Polycomb Repressive Complex 2 Subunit Enhancer of Zeste 2 (EZH2), and found that interactions between SP140 and TOP1 or TOP2A were diminished (Figure 3G) when H3K27me3 was reduced.

SP140 shields TOPs from heterochromatin

To gain insight into how SP140 prevents TOP activity, we assessed TOP1 and TOP2 association with chromatin when SP140 protein levels were perturbed using a previously established TOP chromatin association biochemical assay (Dykhuizen et al., 2013). Here, we found that SP140 shields TOP1 and 2 from association with chromatin, such that less TOP1 and TOP2 remained associated with chromatin after high salt wash in cells overexpressing SP140 compared with vector control cells (Figure 4A). Reduced binding of TOP1 or 2 to chromatin in the presence of SP140 would be expected to compromise function and could represent an inability of TOP1 or TOP2 to associate with substrate DNA. Moreover, TOP1 and TOP2A genome-wide occupancy in primary human macrophages, as assessed by cleavage under targets and tagmentation (CUT&Tag), revealed a preferential gain of both TOP1 and TOP2 at H3K27me3 rich regions upon KD of SP140 (Figures 4B–4D), such as developmentally silenced loci *HOXA7* and *FOXF1* (Figure 4E). Furthermore, GO biological processes and epigenomics roadmap signatures of the loci with enhanced TOP1 and TOP2A occupancy upon SP140 KD reflected those regulating cell fate and identity and associated with markers of heterochromatin, H3K27me3 and H3K9me3 (Figures 4F–4I). TOP1 can occupy transcriptionally silent regions, but this is reduced compared with transcriptionally active regions (Baranello et al., 2016), and TOP2 acts to resolve facultative heterochromatin structure (Miller et al., 2017). Our data reveal SP140 as gatekeeper of TOP activity by physically shielding TOP1 and TOP2 preferentially from these locations. Loss of SP140 leads to enhanced TOP interaction with heterochromatic regions, aberrantly increased chromatin accessibility (Mehta et al., 2017) and depressed transcriptional activity and/or transcriptional potential at these normally silenced regions.

TOP inhibitors rescue defective macrophage cytokine production and bacterial killing upon SP140 knockdown

The *ex vivo* reversal of TOP activity with TPT provided proof of concept for use of TOP inhibitors in SP140-deficient cells. We therefore next explored the use of TOP inhibition to rescue defective innate immune transcriptional programs driven by loss of SP140 (Mehta et al., 2017) and a key driver of disrupted immune-microbiome interactions in inflammatory bowel disease (Blander et al., 2017; Graham and Xavier, 2020). TOP1 inhibitor TPT is used clinically for treatment of small cell lung cancer and cervical cancer (Horita et al., 2015), whereas ETO is approved for treatment of refractory testicular tumor and small cell lung cancer (Loehrer, 1991). However, lower doses of TOP inhibitors can successfully modulate microbe-inducible gene transcription and inflammation *in vivo* (Ho et al., 2021; Rialdi et al., 2016), as well as Aire-dependent immunological tolerance (Bansal et al., 2017). Treatment of SP140 KD primary human macrophages with TPT or ETO reduced inappropriate overexpression of *HOXA9* and *PAX5* at baseline (Figures 5A–5D) and also restored impaired transcription of cytokines *IL6* or *IL12B* in response to LPS (Figures 5E and 5F). Moreover, KD of RNA splicing factors DDX27, DHX30, and NOP56, found to also interact with SP140, did not restore *HOX* or cytokine expression in SP140 KD macrophages (Figures S6A and S6B, related to Figure 5) indicating a specific reliance on TOPs for SP140 regulation of these transcripts. In addition, human SP140 KD macrophages displayed impaired antimicrobial activity toward CD-associated adherent invasive *E. coli*, *C. rodentium*, or *S. typhimurium* as assessed by gentamicin protection assays (Figures 5G–

5I). This microbial killing defect in the absence of SP140 was downstream of depressed developmentally silenced genes such as *HOXA9* (Figure 5J) and was also successfully rescued by TOP 1 or 2 inhibitors (Figures 5G–5I).

TOP inhibitors rescue defective innate immune transcriptional programs in SP140 loss-of-function CD patients

We next exposed PBMCs taken directly from CD patients bearing wild-type (WT) or CD-associated SP140 mutations to TPT or ETO. Fitting with enhanced TOP1 activity, more genes were responsive to TPT activity in SP140 loss-of-function cells than WT cells (Figure 5K), likely reflecting a new chromatin signature susceptible to TOP inhibition (Rialdi et al., 2016) upon loss of SP140. TPT or ETO delivery suppressed inappropriate upregulation of multiple genes in SP140 mutant PBMCs including *LINC000475*, *RASIP1*, *PHLDA2/3*, and *PAX5/8* but, importantly, also restored expression of inducible cytokines including *IL6, IL36G, IL12B, IL23A, TNF,* and *IL1A* back to WT levels (Figure 5L). In fact, TPT or ETO rescued expression of ~50% or ~40% of aberrantly upregulated or downregulated genes in SP140 mutant CD patient PBMCs, respectively (Figure 5M). Importantly, the upregulated lineage-inappropriate genes in SP140 mutant PBMCs were those genes with a higher likelihood of being normally occupied by SP140 (Figure 5N; Mehta et al., 2017). However, downregulated genes such as inducible cytokines were less likely to be occupied by SP140, suggesting an indirect effect of SP140 loss of function on these genes (Figure 5N). Furthermore, those genes whose irregular expression was rescued by TPT or ETO in CD SP140 mutant PBMCs were more likely to be normally occupied by SP140 (Figure 5N). Similarly, TPT or ETO target genes in SP140 mutant PBMCs were also more likely to reside in heterochromatin marked by H3K27me3 (Figure 5O). Consistently, unchecked TOP activity and rescue of this activity in SP140 mutant PBMCs from CD patients with TOP inhibition occurs at loci normally occupied and repressed by SP140 within facultative heterochromatin.

Precision rescue of exacerbated intestinal inflammation due to Sp140 loss with TOP inhibitors

Defective innate immunity and bacterial killing by resident tissue macrophages is a hallmark feature of inflammatory bowel disease (Graham and Xavier, 2020; Peloquin et al., 2016). $Sp140^{-/-}$ mice had significantly exacerbated DSS-colitis compared with WT controls, as measured by weight loss over time (Figure 6A), reduced colon length, and increased interleukin (IL)-6 and TNF in supernatants of colon explants (Figures 6A–6D). These results were confirmed by histological analysis (Figure 6E) and are consistent with previous data using shRNA-mediated Sp140 KD mice (Mehta et al., 2017). Remarkably, administration of WT macrophages to Sp140 deficient animals was able to revert the exacerbated DSS-colitis, indicating that Sp140 deficiency specifically in macrophages is the major driver of colitis (Figures 6A–6E). We therefore next examined the ability of TOP1 or TOP2 inhibition to rescue these macrophage defects for the treatment of inflammatory bowel disease associated specifically with loss of Sp140. Similar to primary human macrophages, Sp140 deficient-bone marrow-derived macrophages displayed impaired bacterial killing against *E. coli*, *C. rodentium* or *S. typhimurium* that was restored with addition of TPT, ETO, or their combination (Figures 6F–6H). Furthermore, intraperitoneal administration of

single or combined TPT and ETO (1 mg/kg each) delivered every other day significantly and specifically alleviated weight loss, rescued tissue architecture, edema and leukocyte infiltration, and reverted colon length in $Sp140^{-/-}$ mice (Figures 6I–6K). In addition, markers of intestinal inflammation, including fecal lipocalin-2 and interleukin (IL)-6 and TNF in supernatants of colon explants of $Sp140^{-/-}$ mice, were all restored with TOP inhibitor administration (Figures 6L–6N). TOP1 or TOP2 inhibitors had no effect on the severity of DSS-colitis in WT mice (Figures 6F–6N), further demonstrating an enhanced effectiveness of TOP inhibitors in the context of SP140 deficiency.

DISCUSSION

Mutations in chromatin reader SP140 are associated with at least three human immune-mediated diseases (International Multiple Sclerosis Genetics et al., 2013; Jostins et al., 2012; Sillé et al., 2012), as well as *Mycobacterium tuberculosis* susceptibility (Ji et al., 2021; Pan et al., 2005), directly implicating it in immunoregulation. Despite this, mechanistic insight into SP140 function in health or disease are limited. Here, we have identified a critical functional role for SP140 in the prevention of DNA accessibility and transcription by repressing and shielding TOPs at heterochromatin. Applying a combination of human genetics, proteomics, biochemistry, and utilization of primary immune cells from CD individuals and *in vivo* animal studies, our study highlights the power of examining human disease-associated mutations to advance mechanistic understanding of chromatin regulators in healthy and disease states. Thus, SP140 maintains inappropriate gene silencing stabilizing both immune cell identity and inducible innate immune transcriptional programs.

To define the SP140-interactome, we characterized the protein complexes associated with SP140 in HEK293T and patient LBL cells. The predominant protein interactors of SP140 were determined to be DNA unwinding and chromatin remodeling proteins including TOP1, TOP2A, TOP2B, DNA-PK, FACT components SUPT16H and SSRP1, as well as SMARCA5. We uncovered a prominent role of SP140 as a negative regulator of TOP1 and 2, and inhibition of either TOP restored derailed transcription due to SP140 loss. Our previous studies revealed SP140 occupancy significantly correlated with the facultative heterochromatin marker, H3K27me3, in primary human macrophages. Loss of SP140 led to increased chromatin accessibility and expression of inappropriate lineage genes such as homeobox (*HOX*)*A9* that impair the functional response of differentiated macrophages (Mehta et al., 2017). Taken together, we propose a model in which SP140, through its recognition of modified histones by its PHD and BRD ‘‘reader’’ modules, interacts with DNA unwinding and chromatin remodeling proteins such as TOPs to shield them from, and prevent chromatin remodeling and transcription, at facultative heterochromatin. This function of SP140 maintains gene silencing and safeguards the differentiated immune cell state and appropriate responses to environmental cues. Notably, this function of SP140, is in contrast to the well-characterized and homologous chromatin reader, Aire which acts to promote transcription via TOPs (Abramson et al., 2010; Bansal et al., 2017). Moreover, SP140 is one of few endogenous proteins characterized to date that negatively regulate TOPs to the best of our knowledge (Andersen et al., 2002; Kobayashi et al., 2009). Our findings further reinforce the importance of chromatin regulatory proteins in silencing lineage-specifying transcription factor genes to maintain a functional cell state (Becker et al.,

2016). We further speculate that this SP140-dependent TOP regulation is a requirement in macrophages due to their unique mobility and responsiveness to stimuli while detecting and adapting to environmental cues.

Innate immune cells, especially intestinal macrophages and intestinal epithelial cells (IECs), support microbial balance, barrier integrity, and tissue repair while maintaining intestinal homeostasis. Moreover, epigenetics is a major mechanism by which these cells integrate microbial and environmental cues to elicit these functions (Amatullah and Jeffrey, 2020). Consistently, chromatin regulator Bap180/Baf180 (subunit of the chromatin-remodeling SWI/SNFcomplex) acts as a conserved transcriptional repressor for maintenance of innate immune homeostasis in the intestine (He et al., 2017). Moreover, histone deacetylase, (HDAC)3, is essential for integration of the host IEC response to diverse microbial and metabolic cues for intestinal homeostasis (Alenghat et al., 2013; Wu et al., 2020). Our studies now ascribe a function for epigenetic reader SP140 in chromatin-mediated gene silencing within innate immune cells for lineage-defining and inducible transcriptional programs that is critical in human immune-mediated disease. Defective innate immunity upon SP140 loss is consistent with multiple studies that revealed a dysfunctional innate immunity as a driver of impaired bacterial sensing and clearance and susceptibility to intestinal inflammation (Burgueño and Abreu, 2020; Fukata et al., 2005; Hu et al., 2015; Lassen et al., 2014; Rakoff-Nahoum et al., 2004; Ramanan et al., 2014). Indeed, genome-wide association studies (GWASs) have identified loss-of-function mutations in multiple innate immune pathways (e.g., NOD2, ATG16L1, and AIM2) as risk factors for inflammatory bowel disease (IBD) (Graham and Xavier, 2020; Peloquin et al., 2016) further emphasizing functional innate immune responses in the gut for normal host-commensal relationships and intestinal homeostasis. Sp140 deficiency was recently shown to result in elevated type I IFN *in vivo* leading to increased susceptibility to *M. tuberculosis* and *L. pneumophila* infection (Ji et al., 2021). It is appealing to speculate that this elevated type I IFN is due to accumulating double-stranded DNA (dsDNA) breaks (Brzostek-Racine et al., 2011; Härtlova et al., 2015) resulting from hyper-active TOPs in the absence of SP140.

Although loss of SP140 resulted in unleashed TOP activity and impaired macrophage function, TOP inhibition effectively restored transcriptional homeostasis and protected $SP140^{-/-}$ mice during DSS-colitis *in vivo*. Intriguingly, DSS-colitis in WT animals was unaffected by TOP inhibition, despite TOP inhibitors attenuating acute inflammation in models of sepsis and COVID (Ho et al., 2021; Rialdi et al., 2016). It is established that a major determinant of action of TOP inhibitors is chromatin state (Ho et al., 2021; Rialdi et al., 2016). Thus, we propose that in the context of SP140 deficiency, TOP inhibitors are specifically redirected to derepressed lineage inappropriate genes because of their enhanced chromatin accessibility and gained TOP occupancy. Furthermore, there are multiple examples where inhibition of innate immune components and cytokines has demonstrated therapeutic benefit in sepsis and other acute inflammation models but showed little effect, or even exacerbated, IBD in mouse models and in clinical trials (Choy et al., 2020; Friedrich et al., 2019), further emphasizing the importance of a functional innate response for intestinal homeostasis. More characterization of TOP inhibition directly in SP140-mutant CD patients will be important for establishing the clinical impact of our work.

Finally, there is significant interest by the global research community in developing small molecule inhibitors of chromatin readers. However, a poorly understood feature of many chromatin ‘readers’ is how specificity of function is achieved through their interaction in multi-protein complexes and how this can be leveraged for therapeutic benefit when their loss-of-function drives disease. Moreover, although oncogenic outcomes are frequently reported (Filippakopoulos et al., 2010; Wan et al., 2020; Wen et al., 2014), human immune pathologies resulting from mutated chromatin regulators are less defined. Collectively, this work expands our knowledge of the types of human diseases that are caused by ‘‘misreading’’ histone modifications. Furthermore, it reveals a mechanism-based strategy to rescue loss-of-function SP140 in human immune disease. CD remains incurable by surgical or therapeutic interventions; hence, future studies may examine a precision-guided approach of FDA-approved TOP inhibitors for the treatment of CD, and potentially MS and CLL patients with loss of SP140, as well as examine potential roles of SP140 in metabolism and RNA processing.

Limitations of the study

Interactions between SP140 and chromatin remodeling and DNA unwinding proteins such as TOPs were lost in SP140 mutant immune cells, but a gain of interactions between SP140 and multiple RNA processing-related proteins was observed. These results indicate that the loss of SP140 in immune disease does not just result in diminishment of the SP140 interactome but rather a functional rewiring of the SP140 interactome is apparent. The importance of RNA processing and how it may influence RNA splicing and generation of alternative transcripts in SP140-driven disease remains an important avenue to be investigated further. Aire, similarly, complexes with RNA processing proteins and influences alternative splicing of its target genes (Abramson et al., 2010). Moreover, whether SP140 operates in a similar fashion in B cells, and if unleashed, TOP activity is a driver of CLL or MS upon SP140 loss of function warrants investigation. Future studies should also examine the role of other SP140 interactors identified in our MS for regulation of transcription including chromatin remodeler SMARCA5 and the FACT complex. LPS-stimulated PBMCs from CD patients with WT or mutant SP140 were subjected to unbiased bulk-RNA-seq and blinded bioinformatic analysis, but sample size was limited to the MGH cohort. Additional experiments testing SP140 KD experiments were consistent with SP140 mutant data. Follow-up work should expand to more CD patient numbers from other patient cohorts and to SP140 loss-of-function patients of other ethnicities and explored in other diseases associated with SP140 loss-of-function mutations. Moreover, since CD-associated SP140 variants trigger altered mRNA splicing and splicing is cell-type dependent, it would be pertinent to examine which cell types, including macrophage subpopulations, within the intestine of $SP140^{mut}$ patients lose SP140 protein most prominently.

STAR★METHODS

RESOURCE AVAILABILITY

Lead contact—Further information and requests for resources and reagents should be directed to and will be fulfilled by the lead contact, Kate L. Jeffrey (kjeffrey@mgh.harvard.edu)

Materials availability—All reagents generated in this study are available from the lead contact with a completed Materials Transfer Agreement.

Data and code availability

- RNA-seq, CUT&Tag, and MINT ChIP data have been deposited at GEO and are publicly available as of the date of publication. RNA-seq data have been deposited in the NCBI Gene Expression Omnibus (GEO) under accession GSE161031. TOP1 and TOP2A CUT&Tag data have been deposited in the NCBI Gene Expression Omnibus (GEO) under accession GSE174466. The H3K27me3 MINT ChIP data has been deposited in the NCBI Gene Expression Omnibus under accession GSE178632. There are no restrictions on data availability. These accession numbers are also listed in the key resources table.
- This paper does not report original code.
- Any additional information required to reanalyze the data reported in this paper is available from the lead contact upon request.

EXPERIMENTAL MODEL AND SUBJECT DETAILS

Human Subjects—Healthy human Peripheral Blood Mononuclear Cells (PBMCs) were isolated from 20–30 mL of blood buffy coats from human volunteers (Blood Components Lab, Massachusetts General Hospital). All patient blood samples were collected under Institutional Review Board (IRB)-approved protocol by Massachusetts General Hospital (MGH) from patients that were enrolled in the ‘‘Prospective Registry in IBD Study at Massachusetts General Hospital (PRISM, IRB# FWA00003136) and genotyped by CD-risk SP140 SNPs rs28445040 and rs6716753 Study research coordinators obtained consent and medical history and data was confirmed by review of the electronic medical record. Patient metadata is provided in Data Table S2. Briefly, mononuclear cells were isolated by density gradient centrifugation of PBS-diluted buffy coat/blood (1:2) over Ficoll-Paque Plus (GE Healthcare). The PBMC layer was carefully removed and washed 3 times with PBS. In order to differentiate into macrophages, PBMCs were re-suspended in X-VIVO medium (Lonza) containing 1% penicillin/streptomycin (Gibco) and incubated at 37°C, 5% CO_2 for 1h to adhere to the tissue culture dish. After 1h, adherent cells were washed 3 times with PBS and differentiated in complete X-VIVO medium containing 100 ng/mL human M-CSF (Peprotech) for 7 days at 37°C, 5% CO_2. On day 4, cultures were supplemented with one volume of complete X-VIVO medium containing 100 ng/mL human M-CSF. 1 million PBMCs or mature macrophages were plated and pretreated with DMSO, topotecan (100nM) or etoposide (25μM) for 1 hour prior to 0.1mg/mL LPS treatment for 4 hours.

Mice—All mice were housed in specific pathogen-free conditions according to the National Institutes ofHealth (NIH), and all animal experiments were conducted under protocols approved by the MGH Institutional Animal Care and Use Committee (IACUC), and in compliance with appropriate ethical regulations. For all experiments, age-matched (8–10 week) female mice Sp140 knockout or wildtype controls were used.

Cells and treatments—HEK293T cells were maintained in DMEM media (Life Technologies) with 1% penicillin-streptomycin (Gibco) and 10% heat-inactivated Hyclone fetal bovine serum (FBS, GE Healthcare). THP-1 human monocytes were maintained in RPMI media (Life Technologies) with 1% penicillin-streptomycin (Gibco) and 10% heat-inactivated Hyclone fetal bovine serum (FBS, GE Healthcare).

METHOD DETAILS

Plasmids—Full-length cDNA encoding human SP140 was amplified from LPS-stimulated primary human peripheral blood derived macrophages. A plasmid expressing SP140 was made by cloning the purified SP140 cDNA into the p3xFLAG-CMV-10 vector (Addgene) using Gateway techniques (Invitrogen). SP140 mutants lacking DNA binding SAND domain (amino acids 580–661, SP140ΔSAND), or chromatin reading Plant homeobox domain (amino acids 690–736 PHD, SP140ΔPHD), Bromodomain (amino acids 746–865, SP140ΔBromo), or CARD domain (amino acids 22–138, SP140ΔCARD), Intrinsically Disordered Region (amino acids 219–413, SP140 ΔIDR), Exon 7 (amino acids 222–247, SP140ΔExon 7), and Exon 11 (amino acids 353–386, SP140ΔExon 11) were generated by overlap-extension PCR using Phusion HF polymerase (Thermo Fisher Scientific). Human SP140 K762A point mutations were introduced via site-directed mutagenesis using QuikChange II (Agilent). HA-Aire plasmid was obtained from Sun Hur (Boston Children's Hospital, Harvard Medical School).

siRNA-mediated knockdown in human macrophages and HEK293T—THP-1 human monocytes or mature primary human peripheral blood derived macrophages were transfected with control (D-001810-10-05, Dharmacon) or SP140 (L-016508-00-0005, Dharmacon) SMARTpool siRNA (100nM) using HiPerfect reagent (Qiagen) or RNAiMAX (Invitrogen) for 48 hours followed by 4 hour LPS treatment (0.1mg/mL). HEK293T cells were used for knockdown experiments with 100nM of Topoisomerase 1 siRNA (siGENOME SMARTpool Human TOP1, M-005278-00-0005, Dharmacon), Topoisomerase 2a siRNA (siGENOME SMARTpool Human TOP2A, M-004239-02-005, Dharmacon), DNA-PK siRNA (siGENOME SMARTpool Human PRKDC, M-005030-01-0005, Dharmacon) and Control (siGENOME Non-Targeting siRNA Pool #1, D-001206-13-05). For double knockdown experiments, primary human peripheral blood derived macrophages were incubated with additional siRNAs: HOXA9 (Human HOXA9 siRNA, L-006337-00-005, Dharmacon) DDX27 (Human DDX27, L-013635-01-0005, Dharmacon), DHX30 (Human DHX30, L-017196-01-0005) and NOP56 (Human NOP56, L-019143-01-005, Dharmacon).

Generation of CRISPR-mediated Sp140 null macrophages—Immortalized Cas9 overexpressing bone marrow-derived mouse macrophages were a kind gift from Dr. Kate Fitzgerald (University of Massachusetts Medical School). Mouse guide RNA sequences against SP140 were designed using Broad Institute's sgRNA design algorithm (https://portals.broadinstitute.org/gpp/public/analysis-tools/sgrna-design). Guide 1 (TGTTGGGGAACATATGACAC) and Guide 2 (AAGGAAAAATTCAAACAAGG) sequences were cloned into lentiGuide-puro plasmid (Addgene, #52963), transformed in Stbl3 bacteria (Invitrogen, C7373-03), and subsequently purified with Qiagen Miniprep

Kit. LentiGuide-Puro empty vector (control) or SP140 gRNA cloned plasmids were then co-transfected into HEK293T cells with the packaging plasmids pVSVg (AddGene 8454) and psPAX2 (AddGene 12260) for generation of lentivirus particles. Cas9 immortalized macrophages were transduced with lentivirus particles and 48 hours later treated with puromycin. Single cell clones were subsequently picked and grown.

Generation, characterization and testing of hiPSC-derived M(IFNγ) macrophages—Human induced pluripotent stem cell lines (hiPSC), derived from three patients with Crohn's Disease (CD) homozygous for the CD-associated minor allele of the rs28445040 variant in SP140 ($SP140^{mut}$) and from three healthy controls (HC) homozygous for the major allele ($SP140^{wt}$) were produced through reprogramming of lymphoblastoid cell lines (LCL). HiPSC lines were then differentiated into CD14+ monocytes and validated via FACS analysis. Harvested monocytes were further cultured and differentiated into M0 macrophages by adding M-CSF for 7 days, and then polarized to M1 macrophages with IFNγ.

Lymphoblastoid B cell lines (LBLs) reprogramming into hiPSCs: Human lymphoblastoid cell lines (LBL) collected by the NIDDK IBD Genetics Consortium from three patients with Crohn's Disease (CD) homozygous for the CD-associated minor allele of the rs28445040 variant in SP140 ($SP140^{mut}$) and from three healthy controls (HC) homozygous for the major allele ($SP140^{wt}$) were obtained from the NIDDK Central Repository (https://repository.niddk.nih.gov).

Patient information:

CD/HC	Sex	Genotype at rs28445040	Label	Age
HC	F	C/C	$SP140^{wt}$	35
HC	M	C/C	$SP140^{wt}$	65
HC	M	C/C	$SP140^{wt}$	70
CD	F	T/T	$SP140^{mut}$	23
CD	M	T/T	$SP140^{mut}$	35
CD	M	T/T	$SP140^{mut}$	37

LBL reprogramming was performed as described by Kumar et al. (27375745). Briefly, $1x10^6$ cells were nucleofected with four episomal reprogramming plasmids (pCE-hUL, pCE-hSK, pCE-hOCT3/4, and pCE-mp53DD) using the Amaxa® Human Monocyte Nucleofector® Kit (Lonza) according to the manufacturer's protocol. After an 8-12 hours recovery period in complete media (RPMI1640-GlutaMAX™ (Life Technologies) supplemented with 20% FBS (Sigma Aldrich) and 1% P/S (Wisent), the cells were transferred to Matrigel® (Corning) coated plates in TeSR™-E7™ (STEMCELL™ Technologies) reprogramming media. Cell were then cultivated for 13 to 15 days, and when hiPSC-like colonies started to appear, the growth media was changed to Stemflex (Gibco™). Colonies were tested for TRA-1-60 expression between days 20 and 22, and four TRA-1-60 colonies were picked and expanded for each cell lines. Each hiPSC cell line was then further

sub-cloned by sorting of single cells into single wells of Matrigel®-coated 96-well plates containing Stemflex media supplemented with 1X Revitacell (Gibco™) using a FACSAria Fusion (BD Biosciences) cell sorter. Media was changed every 3–4 days and the amount of Revitacell was reduced to 1/2X after 6 days. Each well was investigated for the emergence of colonies derived from single cells and 2 sub-clones of each cell line were selected, characterized, and expanded for further studies after 11–12 days.

hiPSC characterization: Each hiPSC sub-clonal line was then tested for the absence of genomic integration of the four plasmids used for LBL-hiPSC reprogramming via a PCR amplification of plasmid DNA using HotStarTaq Plus DNA Polymerase (Qiagen). The hiPSC lines were also tested for the expression of pluripotency markers NANOG, SOX2 and POU5F1 by RT-qPCR amplification. Finally, the capacity of each of these sub-clonal hiPSC lines to differentiate into the three germ layers was assessed using the Human Pluripotent Stem Cell Functional Identification Kit (R&D Systems) following manufacturer's instructions.

Differentiation of hiPSCs into monocytes: The differentiation of hiPSC lines into monocytes was performed as described by Yanagimachi, M. D. et al. (23573196). Briefly, 30 colonies obtained using the ReLeSR™ solution (STEMCELL™ Technologies) were seeded in a 100mm Petri dish containing mTeSR1 STEMCELL™ Technologies) medium. At Day 0, BMP4 (Sigma Aldrich, 80 ng/mL) was added to the mTeSR1 medium. Between Days 4 and 5, medium was changed to Stempro®-34 SFM (1X) (Gibco™) supplemented with VEGF (Sigma Aldrich, 80 ng/mL), bFGF (Sigma Aldrich, 25 ng/ml), and SCF (Sigma Aldrich, 100 ng/mL) to promote the development of hemoangiogenic progenitors. On Days 6 and 7, the cytokine cocktail was changed to SCF (50 ng/mL), IL-3 (R&D systems, 50 ng/mL), TPO (Thrombopoietin) (Sigma Aldrich, 5 ng/mL), M-CSF (Sigma Aldrich, 50 ng/mL), and Flt-3 ligand (Sigma Aldrich, 50 ng/mL) for the generation of hematopoietic cells. Finally, the cytokine cocktail was changed to Flt-3 ligand (50 ng/mL), GM-CSF (Sigma Aldrich, 25 ng/mL), and M-CSF (50 ng/mL) between Days 13 and 15 to drive the monocytic lineage-directed differentiation. Following that, free floating monocytes were harvested from the supernatant and the medium was changed every 3–4 days. Monocytes were first visualized using H&E staining. Briefly, 50,000 monocytes were collected and laid on a polarized microscope slide (Thermo Fisher Scientific) and allowed to dry completely. Then, slides were fixed and stained following manufacturer's instructions (Hema 3™ Manual Staining System and Stat Pack, Thermo Fisher Scientific).

The production of CD14+ monocytes was confirmed through FACS analysis. Briefly, a minimum of 50,000 cells were harvested from the supernatant of monocyte differentiation cultures and washed in cold sorting buffer. Cells were blocked by incubating 20 mL of FcR Blocking Reagent (MACS Miltenyi Biotec) for 10 min at 4°C prior to antibody staining. The antibody used was the BV421 Anti-Human CD14 (Clone M5E2) (BD Biosciences). Cells were incubated with the antibody 30 min at 4°C and then washed twice with cold sorting buffer. Cells were filtered using 70μM Pre-Separation Filters (MACS Miltenyi Biotec). Control was made with the appropriated isotype control and viability was assessed by

7-AAD staining solution (BD Biosciences). CD14+ staining was measured on a FACS Aria Fusion and analyzed using FlowJo™ software.

Differentiation of monocytes into activated M(IFNγ) macrophages: The differentiation of harvested monocytes into M1 macrophages was performed as described by Yanagimachi, M. D. et al. (23573196). Briefly, 300,000 CD14+ monocytes were plated in a 24-well plate and cultured for 7 days in RPMI1640-GlutaMAX™ (Life Technologies) supplemented with 10% FBS and M-CSF (100ng/ml). Differentiated M0 macrophages were visualized using H&E staining. For this purpose, 100,000 CD14+ monocytes were plated in Cell Imaging Coverglass (Eppendorf). On Day 7, cells were fixed and stained with the Hema 3™ Manual Staining System and Stat Pack, following manufacturer's instructions. Subsequent polarization of macrophages was achieved via the addition of IFNγ (20 ng/ml) to the media for 24h followed by 4h of LPS (Lippopolysaccharide from Escherichia coli O111:B4, Sigma Aldrich, 100ng/ml) treatment to activate the M1 macrophages. The differentiation of CD14+ monocytes into M1 macrophages was confirmed through FACS analysis. Briefly, a minimum of 100,000 M1 macrophages were harvested using Stempro Accutase (Thermo Fisher Scientific) for 10 min at 37°C and washed in cold sorting buffer. Cells were blocked by incubating 20 mL of FcR Blocking Reagent (MACS Miltenyi Biotec) for 10 min at 4°C prior to antibody staining. The antibody used was the BUV737 Anti-Human HLA-DR (Clone G46-6) (BD Biosciences). Cells were incubated with the antibody 30 min at 4°C and then washed twice with cold sorting buffer. Cells were filtered using 70μM Pre-Separation Filters (MACS Miltenyi Biotec). Control was made with the appropriated isotype control and viability was assessed by 7-AAD staining solution (BD Biosciences). HLA-DR+ staining was measured on a FACS Aria Fusion and analyzed using FlowJo™ software.

Quantitative PCR—RNA was extracted using the RNeasy Mini Kit (Qiagen) with on-column DNase digest (Qiagen)according to manufacturer's instruction. 100ng-1μg RNA was used to synthesize cDNA by reverse transcription using the iScript cDNA Synthesis Kit (Bio-Rad). Quantitative PCR reactions were run with cDNA template in the presence of 0.625μM forward and reverse primer and 1x solution of iTaq Universal SYBR Green Supermix (Bio-Rad). Quantification of transcript was normalized to the indicated housekeeping gene. A complete list of primer sequences is provided in STAR Methods chart.

Mass Spectrometry—HEK293T cells were transfected with FLAG-Empty Vector (FLAG-EV) and FLAG-SP140 plasmids using Lipofectamine 2000 (Invitrogen) for 48 hours. Lysates were incubated with FLAG M2 (Sigma, F3165) antibody and immunoprecipitated protein was run on a 4–12% Tris-Bis. Gel and stained with Silver Stain (Thermo Fisher) and gel sections were cut and sent for in-gel digestion, micro-capillary LC/MS/MS, analysis, protein database searching and data analysis at the Taplin Mass Spectrometry Facility (Harvard Medical School). Mass Spec of lymphoblastoid cells (LBLs) carrying SP140 wildtype or SP140 loss-of-function variants (homozygous for rs7423615, Coriell Institute of Medical Research) was performed on endogenous SP140 immunoprecipitated from 1mg of nuclear lysates with SP140 antibody (Sigma).

Nuclear fractionation—Cells were washed in PBS and gently lysed by resuspension in a freshly prepared and chilled sucrose lysis buffer (320 mM sucrose, 10 mM Tris pH 8.0, 3 mM $CaCl_2$, 2mM magnesium acetate, 0.1 mM EDTA, 0.5% NP-40, 1% protease/phosphatase inhibitor cocktail). Cells were incubated in this buffer for 15 minutes on ice followed by centrifugation at 500*g* for 15 minutes at 4°C to pellet isolated nuclei. Supernatant containing the cytosolic fraction was removed and the remaining nuclear pellet was mixed in a nuclei sonication buffer (500 mM NaCl, 50 mM Tris pH 8.0, 10% glycerol, 1% NP-40, 1% protease/phosphatase inhibitor cocktail) followed by incubation on ice for 5 minutes. Next, the nuclei were lysed in this buffer by sonication for 10 seconds. Insoluble debris from this lysate was removed by centrifugation at 21000*g* for 20 minutes at 4°C and remaining supernatant was taken as nuclear fraction protein.

Chromatin Association Assay—For chromatin fractionation, $1x10^7$ cells were washed with PBS and resuspended in 200μL of Buffer A (10mM HEPES (pH 7.9), 50mM NaCl, 0.5M sucrose, 0.1mM EDTA, 1mM dithiothreitol, 1% NP40 and protease inhibitor (Roche)). The cells were incubated on ice for 5 min and subsequently nuclei were pelleted by centrifugation at 3,000 rpm for 10 min at 4°C. The cytoplasmic fraction was removed and the pellet was washed once with Buffer A then lysed in 200μL of Buffer B (10mM HEPES (pH 7.9), 150mM NaCl, 0.1mM EDTA, 1mM dithiothreitol, 1% NP40 and protease inhibitor mixture), followed by 10-min incubation on ice. Soluble nuclear proteins were separated from chromatin by centrifugation (5,000 r.p.m., 5min). The pellet was solubilized using sonication in Buffer C (10mM HEPES (pH 7.9), 0.1mM EDTA, 1% NP40 and 1mM dithiothreitol, protease inhibitor with either 150mM NaCl, 300nM NaCl or 600nM NaCl) and the association of different proteins to chromatin was analyzed using Western blotting.

Co-immunoprecipitation—HEK293T cells were seeded into 10-cm dishes and transfected with 25μg FLAG-Empty Vector (FLAG-EV) and FLAG-SP140 plasmids using Lipofectamine 2000 (Invitrogen). 48 hours after transfection, nuclear extracts were isolated from cells. Alternatively, nuclear extracts from 10 million THP1 monocyte, peripheral blood mononuclear cells (PBMCs) or LBL cells were used for endogenous SP140 IPs. 500μg of nuclear lysate was incubated with SP140 antibody (Sigma) for pulldown overnight at 4°C. This was followed by addition of Protein G Dynabeads (Invitrogen) and incubation for 4 hours at 4°C with rotation. The bead slurry was then magnetized, the unbound fraction removed, and the beads subjected to a series of increasingly harsh salt-based washes. The beads were boiled at 90°C for 10 minutes in a reducing sample buffer to elute bound protein and the elution was used for probing of co-IP interactors by Western blotting. Eluted proteins were run on a 3–8% Tris Acetate Gel (Invitrogen) or 4–12% Tris Bis gel (Invitrogen), transferred onto PVDF membrane, blocked with 5% skim milk in TBS/0.1% Tween at room temperature for 1h, and then incubated with the indicated primary antibody in 3% BSA TBS/0.1% Tween overnight at 4°C. To assess DNA dependence of co-IP interactors, ethidium bromide was added at a concentration of 1mg/mL to 500μg of nuclear lysate and allowed to incubate for 30 minutes on ice prior to addition of antibody for pulldown as described previously. Salt-based wash solutions were also supplemented with 100μg/mL ethidium bromide. As before, beads were boiled and eluted protein was used for probing of interactors by Western blot.

Prediction of SP140 SUMOylation sites—Potential sumoylation sites on SP140 protein were predicted and ranked through GPS-SUMO web interface tool http://sumosp.biocuckoo.org/index.php which is based off published algorithms (Ren et al., 2009; Zhao et al., 2014). Position 762 with a significant P-value was used for subsequent mutagenesis.

Position	Peptide	Score	Cutoff	P-value	Type
50	FRFFRENKVEIASAI	3.339	3.32	0.072	Sumoylated Non-concensus
525	SQQNDNSKADGQVVS	3.783	3.32	0.232	Sumoylated Non-concensus
762	MCPEEQLKCEFLLLK	7.547	2.13	0.016	Sumoylated concensus

Topoisomerase activity assays—Full length human recombinant SP140 protein was commercially produced by BPS Bioscience using a HEK293T expression system. Recombinant Topoisomerase I and II were purchased from Topogen. Nuclear lysates were obtained from control or SP140 knockdown THP-1 cells or primary human peripheral blood-derived macrophages, HEK overexpressing FLAG SP140 or SP140 protein domain mutants, or lymphoblastoid cells (LBLs) carrying wildtype or SP140 genetic variants (homozygous for rs7423615) and Topoisomerase I activity was performed according to the manufacturer's instructions (Topoisomerase I activity assay kit, TopoGen). Briefly, nuclear lysates were incubated with supercoiled plasmid (pHOT) DNA substrate, and reaction buffer (10mM Tris-HCl pH 7.9, 1mM EDTA, 0.15M NaCl, 0.1% BSA, 0.1mM Spermidine, 5% glycerol) for 30 minutes at 37°C. The reaction was stopped using a ''Stop'' Buffer (0.125% Bromophenol Blue, 25% glycerol, 5% Sarkosyl) and samples were treated with proteinase K (50μg/mL) and Ribonuclease A (Roche) for 30 minutes at 37°C to remove contaminating proteins and RNA. The reaction mixture, along with supercoiled and relaxed controls, were then run on a 1% agarose gel, stained with Ethidium Bromide for 20 minutes, de-stained in distilled water, and imaged for photodocumentation. Bands were quantified using Image Studio Lite (Licor Biosciences) and ratios were calculated with relaxed over supercoiled quantified data. Topoisomerase II activity assay was performed according to the manufacturer's instructions (Topoisomerase II activity assay kit, TopoGen). Briefly, recombinant SP140 protein was incubated with recombinant TOP2A protein, catenated plasmid kinetoplast DNA (from insect C *fasciculate*) substrate, reaction buffer (0.5M Tris-HCl pH 8, 1.5M NaCl, 100mM MgCl2, 5mM Dithiothreitol, 300μg/mL BSA) for 30 minutes at 37°C. The reaction was stopped using a ''Stop'' Buffer (0.125% Bromophenol Blue, 25% glycerol, 5% Sarkosyl). The reaction mixture, along with catenated and decatenated circular and linear controls, were then run on a 1% Ethidium Bromide agarose gel, destained in distilled water, and imaged for photodocumentation. Bands were quantified using Image Studio Lite (Licor Biosciences) and ratios were calculated with decatenated relaxed and nicked DNA over catenated quantified data.

Flow Cytometry—Macrophages were fixed as single cell suspensions in 4% formaldehyde. Fixed cells were then permeabilized in 0.25% Triton X-100 and blocked in 1% BSA/0.05% Tween-20 in PBS. Cells were then incubated with 1:500 γH2AX antibody

(Abcam), followed by washing and collection in FACS buffer (1% FBS in PBS) for flow cytometry. Annexin V and propidium iodide for cell death analysis was performed according to manufacturer's instructions (Alexa Fluor® 488 annexin V/Dead Cell Apoptosis Kit, Thermofisher). Cell cycle analysis was performed with ethanol fixed cells and stained in PBS with 50μg/mL Propidium Iodide and 100μg/mL RNase A. All flow cytometry data was collected on LSRII (BD) and analyzed with FlowJo (TreeStar).

Immunofluorescence microscopy—Control or *SP140* siRNA-mediated knockdown THP1 or CRISPR-mediated Sp140 null mouse immortalized bone marrow-derived macrophages were fixed with 4% formaldehyde for 20 mins and subsequently permeabilized with 0.25% Triton X-100, blocked with 5% BSA/PBST and stained with 1:500 γH2AX antibody (Abcam) overnight at 4°C. The samples were subsequently washed the next day and incubated with secondary antibody at 1:1000 (AlexaFluor 488, Invitrogen) for 1 hour at room temperature, following which cells were washed and coverslips were mounted onto microscope slides with Prolong Diamond anti-fade mountant (Invitrogen). Multiple representative images were obtained on a confocal microscope (Zeiss LSM 800 Airyscan). Images were quantified using ImageJ (Schneider et al., 2012) by measuring fluorescence intensity across the diameter of a nucleus of 25 cells. Quantified data were binned to normalize different sized cells and plotted as a lineplot with Python showing average intensity from one periphery of the cell to the other periphery.

Chromatin Immunoprecipitation (ChIP)—Ten million naïve or LPS-stimulated (0.1mg/mL for 4 hours) human peripheral blood-derived macrophages were cross-linked and processed using truChIP kit (Covaris Inc), as described in detail before(Mehta et al., 2017). Input fraction was saved (10%), and the remaining sheared chromatin was used for ChIP with γH2AX antibody (Abcam) or an immunoglobulin G isotype control (Abcam) in immunoprecipitation buffer (0.1% Triton X-100, 0.1 M Tris-HCl pH 8, 0.5 mM EDTA, and 0.15 M NaCl in 1Å ~ Covaris D3 buffer) at 4°C, rotating overnight, followed by incubation with Dynabeads Protein G (Life Technologies) for 4 hours. The chromatin-bead-antibody complexes were then washed sequentially with three wash buffers of increasing salt concentrations and TE buffer. Chromatin was eluted using 1% SDS in Tris-EDTA. Cross-linking was reversed by incubation with ribonuclease A (Roche) for 1 hour at 37°C, followed by an overnight incubation at 65°C with Proteinase K (Roche). DNA was purified with the QIAquick PCR Purification Kit (Qiagen). DNA was used for ChIP qPCR using primers in Extended Table 4. ChIP data across different donors was normalized to γH2AX ChIP of control sample of each donor.

RNA library prep, sequencing and analysis—RNA was extracted using the Qiagen RNeasy Mini Kit (with on-column DNase I digest) and samples were eluted in 40μL RNase-free water. Sample concentration and quality was measured using the HighSensitivity RNA TapeStation kit for the TapeStation Bioanalyzer (Agilent). After confirming the RNA was of sufficient quality using the RIN^e metric, 100ng of RNA was taken from each sample and made up to 50μL in RNase-free water. mRNA was enriched for and used to prepare libraries using the NEBnext Poly(A) mRNA magnetic isolation module (NEB E7490S) and NEBnext Ultra II RNA library prep kit (NEB E7770S). Briefly, poly(A)-tailed RNA was isolated by

coupling with Oligo d(T) magnetic beads followed by a series of washes to remove unbound RNA. This coupling was repeated for a total of two selection steps. Finally, beads were resuspended in a mix of random primers and First Strand Synthesis Buffer and boiled for 10 minutes to fragment selected mRNA. First Strand Enzyme mix was added to the fragmented RNA-buffer elution and thermal cycled for preparation of cDNA. The second strand was synthesized in a similar manner, using the respective buffers and enzymes. Double-stranded cDNA was selected for using SPRI size selection magnetic beads, end prepped, and ligated with unique adapters for multiplexing. This ligation mixture was PCR cycled to amplify cDNA and libraries were purified using a series of SPRI size selection steps. Finally, library size and purity were confirmed using the High Sensitivity D1000 Tapestation kit on Tapestation Bioanalyzer. Multiplexed samples were submitted for paired-end sequencing on NovaSeq S2 (Genomics Platform, Broad Institute), resulting in 14–52 million mapped reads per sample. Reads were mapped using the STAR aligner (Dobin et al., 2013) and the hg19 assembly of the human genome. Read counts for individual transcripts were obtained using HTSeq (Anders et al., 2015) and the Ensembl gene annotation (GRCh37 release 75) (Yates et al., 2016). Differential expression analysis was performed using the EdgeR package (McCarthy et al., 2012), and differentially expressed genes were defined based on the criteria of >2-fold change in normalized expression value. For probability density distribution analysis of differential genes, ChIP signal enrichments at promoters were calculated by counting reads in the region defined by ±3 kb from the TSS. Read counts were normalized to reads per million (RPM), and the enrichment was calculated as the ratio of RPM in ChIP divided by the RPM in input chromatin (control) and was converted to $\log_2$ scale. The probability density distribution was computed and plotted with standard R package. SP140 ChIP-seq in primary human macrophages was previously generated in our lab (Mehta et al., 2017) and H3K27me3 analysis included ChIP-seq obtained in peripheral blood mononuclear cells (ENCODE accession: ENCSR553XBX, ENCSR866UQO, ENCSR390SFH. An average of these three studies was used).

Multiplexed indexed T7 ChIP-seq (MintChIP)—To profile H3K27me3 levels in control primary human macrophages, we performed optimized version of Mint-ChIP3 (van Galen et al., 2016), as described before. Briefly, 100,000 cells were lysed and digested with 300 units of micrococcal nuclease (MNase, NEB) for 15 mins. T7 Adapter Ligation was subsequently performed and quenched. All samples were pooled and then equally split for primary antibody (H3K27me3 and H3 Antibody) overnight incubation at 4C. Protein G Dynabeads were added the next morning and incubated for 4 hours at 4°C. Following low salt RIPA, high salt RIPA, LiCl and TE washes, the beads were eluted and digested at 63°C for 1 hour. The beads were cleaned up using AMPure SPRI beads (Beckman Coulter). In vitro transcription of eluted DNA to RNA was performed using NEB HiScribe T7 kit for 2 hours and subsequently treated with DNase at 37°C for 15 mins. RNA was isolated using Silane beads (Thermofisher). RNA was reverse transcribed to cDNA and subsequently cleaned up with AMpure SPRI beds. The purified DNA was then used for Library PCR with Illumina barcoded primers to Enrich Adapter-Modified DNA Fragments. Samples were submitted for sequencing on HiSeq (Genomics Platform, Broad Institute). MINT ChIP reads were aligned to the hg19 genome using BWA version 0.7.15, technical replicates were pooled together. bigWig files were generated using the deepTools bam-Coverage

command, normalized using CPM, and with bin size of 50, and smooth length of 100. Normalized bigWig files were used to calculate intensities at promoters from the Ensembl gene annotation (GRCh37 release 75) using the deepTools multiBigwigSummary command, with a BED file obtained by extending the TSS by +/− 3000 bp.

Cleavage Under Targets and Tagmentation (CUT&Tag)—CUT&Tag was performed according to Epicypher protocol. Briefly, nuclei were isolated from 100,000 primary human macrophages and bound to activated magnetic concanavalin A beads (Epicypher). The bound nuclei were incubated with primary antibody overnight at 4°C. The next day, the beads were washed and subsequently incubated with secondary antibody for 0.5 hour at room temperature. This was followed by washing and incubation with the protein A/G conjugated Tn5 (CUTANA pAG-Tn5, Epicypher) enzyme for one hour at room temperature. The enzyme bound beads were then washed, and then tagmentation reaction was performed for 1 hour at 37°C. The reaction was stopped with TAPS buffer containing EDTA, released with SDS buffer, and quenched with 0.67% Triton X-100 solution. The released DNA was cleaned up using Monarch DNA PCR Clean Kit (NEB) and eluted in TE buffer. Library was constructed using universal i5 and barcoded i7 primers and non-hot start CUTANA® High Fidelity 2x PCR Master Mix (Epicypher). DNA was cleaned and size selected using 1.3x AMPure beads and visualized on Agilent Bioanalyzer system. Samples were submitted for sequencing on the NovaSeq_SP_100 (Genomics Platform, Broad Institute). Paired-end sequencing reads were aligned to hg19 human reference genome using bwa version 0.7.17 (Li and Durbin, 2009). diffBind R package (Ross-Innes et al., 2012) was used for the analysis of differential regions between knockdown and control samples at promoter regions (+/− 3kb proximity of transcription start sites). Differential regions were determined based on the cutoffs of > 2-fold change of read density and false discovery rate (FDR) < 0.01. Heatmaps and metaplots of CUT&Tag signal densities were generated using deepTools (Ramírez et al., 2014).

Gentamicin Protection Assay—Primary human macrophages or bone marrow derived macrophages (1x 10^6) plated in 12-wellplates were infected with live adherent invasive E. coli, C. rodentium, and S. *typhimurium* at a 1:10 with spin infection for 10 mins and incubation for 20 mins. Cells were washed three times with 1x PBS and provided medium containing 100 μg/mL gentamicin for 1 hour. Cells were washed again with 1x PBS and lysed with 0.1% Triton x-100 in 1x PBS following 1, 2 or 3 hours for E. coli, C. rodentium and S. *typhimurium*, respectively. Serially diluted cell lysates were plated on LB agar plates. Colony forming units (CFUs) were determined after 24 hours of incubation at 37°C with 5% CO_2.

Dextran Sodium Sulfate (DSS) colitis—All mice were housed in specific pathogen-free conditions according to the National Institutes ofHealth (NIH), and all animal experiments were conducted under protocols approved by the MGH Institutional Animal Care and Use Committee (IACUC), and in compliance with appropriate ethical regulations. For all experiments, age-matched mice Sp140 knockout or wildtype controls were randomized and allocated to experimental group, with 6–12 mice per group. No statistical method was used to determine sample size. Mice were administered 2.5% Dextran Sodium

Sulfate Salt (DSS, MW = 36,000–50,000 Da; MP Biomedicals) in drinking water *ad libitum* for 7 days (freshly prepared every other day), followed by regular drinking water for 5 days. For macrophage transfer experiments, 7 day mature bone marrow derived macrophages were injected ($1x10^6$, i.v.) one day before DSS administration and Day 4 post DSS. For topoisomerase inhibition experiments, mice were administered DMSO (control), topotecan (Sigma) or etoposide (Sigma) by intraperitoneal injection (i.p. 1mg/kg) starting on day 1 and administered every other day until mice were sacrificed on day 12. Colon length was measured and Day 9 fecal samples were homogenized in PBS, spun down and supernatants were collected and assayed for Lipocalin-2 by ELISA, according to manufacturer's instructions (R&D). For cytokine measurements, day 12 colon tissue (excised approximately 1 cm) was washed in PBS and then placed in a 24 well plate containing 1mL of RPMI medium with 1% penicillin/streptomycin and incubated at 37°C with 5% CO2 for 24 hours. Supernatants were collected and centrifuged for 10 min at 4°C and IL-6 and TNF levels were assessed by ELISA, according to manufacturer's instructions (R&D).

QUANTIFICATION AND STATISTICAL ANALYSIS

Results are shown as mean ± s.e.m. Visual examination of the data distribution as well as normality testing demonstrated that all variables appeared to be normally distributed. Comparisons and statistical tests were performed as indicated in each figure legend. For comparisons of two groups, two-tailed unpaired t tests were used, except where indicated. For comparison of multiple groups, one-way ANOVA was used. Statistical analyses were performed in the GraphPad Prism 8 software. The *P* values denoted throughout the manuscript highlight biologically relevant comparisons. A *P* value of less than 0.05 was considered significant, denoted as $*P<0.05$, $**P<0.01$, $***P<0.001$, and $****P<0.0001$ for all analyses.

Supplementary Material

Refer to Web version on PubMed Central for supplementary material.

ACKNOWLEDGMENTS

Figure schematics were created using Biorender.com. We thank the Taplin Mass Spectrometry Facility of Harvard Medical School, the Massachusetts General Hospital (MGH) Next Gen Sequencing core, the Broad Institute of Harvard and MIT Genomics Platform, the MGH Histopathology Research Core, the Harvard Stem Cell Institute CRM Flow Cytometry Core Facility, and the Microscopy Core of the Program in Membrane Biology (PMB) at MGH. We also sincerely thank Stuti Mehta for initiating Mass Spectrometry experiments, Russell Vance (University of California, Berkeley) for $Sp140^{-/-}$ mice, Kate Fitzgerald (University of Massachusetts Medical School) for immortalized Cas9 transgenic bone marrow-derived mouse macrophages, Maya Kitaoka (Massachusetts General Hospital) for assistance with cloning, and the clinical coordinators and patients enrolled in the Prospective Registry in IBD study at Massachusetts General Hospital (PRISM). We thank Ramnik Xavier and Raul Mostoslavsky for constructive comments. This study was supported by Canadian Institutes of Health Research (CIHR) postdoctoral fellowship (H.A.), F31DK127518 (I.F.), Tier 1 Canada Research Chair (#230625), and the Canada Foundation for Innovation (#202695, 218944, and 20415, J.D.R.). NIH R01AI155662 (R.M.A.), the Kenneth Rainin Foundation Innovator and Synergy Awards (K.L.J.), NIH R01DK119996 (K.L.J.), and K.L.J. is a John Lawrence MGH Research Scholar, 2020–2025. K.L.J. is an employee of Moderna Therapeutics since November 2021 (kate.jeffrey@modernatx.com)

REFERENCES

Abramson J, Giraud M, Benoist C, and Mathis D (2010). Aire's partners in the molecular control of immunological tolerance. Cell 140, 123–135. [PubMed: 20085707]

Alenghat T, Osborne LC, Saenz SA, Kobuley D, Ziegler CG, Mullican SE, Choi I, Grunberg S, Sinha R, Wynosky-Dolfi M, et al. (2013). Histone deacetylase 3 coordinates commensal-bacteria-dependent intestinal homeostasis. Nature 504, 153–157. [PubMed: 24185009]

Amatullah H, and Jeffrey KL (2020). Epigenome-metabolome-microbiome axis in health and IBD. Curr. Opin. Microbiol 56, 97–108. [PubMed: 32920333]

Anders S, Pyl PT, and Huber W (2015). HTSeq–a Python framework to work with high-throughput sequencing data. Bioinformatics 31, 166–169. [PubMed: 25260700]

Andersen FF, Tange TØ, Sinnathamby T, Olesen JR, Andersen KE, Westergaard O, Kjems J, and Knudsen BR (2002). The RNA splicing factor ASF/SF2 inhibits human topoisomerase I mediated DNA relaxation. J. Mol. Biol 322, 677–686. [PubMed: 12270705]

Bansal K, Yoshida H, Benoist C, and Mathis D (2017). The transcriptional regulator Aire binds to and activates super-enhancers. Nat. Immunol 18, 263–273. [PubMed: 28135252]

Baranello L, Wojtowicz D, Cui K, Devaiah BN, Chung HJ, Chan-Salis KY, Guha R, Wilson K, Zhang X, Zhang H, et al. (2016). RNA polymerase II regulates topoisomerase 1 activity to favor efficient transcription. Cell 165, 357–371. [PubMed: 27058666]

Becker JS, Nicetto D, and Zaret KS (2016). H3K9me3-dependent heterochromatin: barrier to cell fate changes. Trends Genet 32, 29–41. [PubMed: 26675384]

Blander JM, Longman RS, Iliev ID, Sonnenberg GF, and Artis D (2017). Regulation of inflammation by microbiota interactions with the host. Nat. Immunol 18, 851–860. [PubMed: 28722709]

Bloch DB, de la Monte SM, Guigaouri P, Filippov A, and Bloch KD (1996). Identification and characterization of a leukocyte-specific component of the nuclear body. J. Biol. Chem 271, 29198–29204. [PubMed: 8910577]

Brzostek-Racine S, Gordon C, Van Scoy S, and Reich NC (2011). The DNA damage response induces IFN. J. Immunol 187, 5336–5345. [PubMed: 22013119]

Buchwalter A, Kaneshiro JM, and Hetzer MW (2019). Coaching from the sidelines: the nuclear periphery in genome regulation. Nat. Rev. Genet 20, 39–50. [PubMed: 30356165]

Bunch H, Lawney BP, Lin YF, Asaithamby A, Murshid A, Wang YE, Chen BP, and Calderwood SK (2015). Transcriptional elongation requires DNA break-induced signalling. Nat. Commun 6, 10191. [PubMed: 26671524]

Burgueño JF, and Abreu MT (2020). Epithelial toll-like receptors and their role in gut homeostasis and disease. Nat. Rev. Gastroenterol. Hepatol 17, 263–278. [PubMed: 32103203]

Choy EH, De Benedetti F, Takeuchi T, Hashizume M, John MR, and Kishimoto T (2020). Translating IL-6 biology into effective treatments. Nat. Rev. Rheumatol 16, 335–345. [PubMed: 32327746]

Cotsapas C, and Hafler DA (2013). Immune-mediated disease genetics: the shared basis of pathogenesis. Trends Immunol 34, 22–26. [PubMed: 23031829]

Dawson MA, Prinjha RK, Dittmann A, Giotopoulos G, Bantscheff M, Chan WI, Robson SC, Chung CW, Hopf C, Savitski MM, et al. (2011). Inhibition of BET recruitment to chromatin as an effective treatment for MLL-fusion leukaemia. Nature 478, 529–533. [PubMed: 21964340]

Dobin A, Davis CA, Schlesinger F, Drenkow J, Zaleski C, Jha S, Batut P, Chaisson M, and Gingeras TR (2013). STAR: ultrafast universal RNA-seq aligner. Bioinformatics 29, 15–21. [PubMed: 23104886]

Dykhuizen EC, Hargreaves DC, Miller EL, Cui K, Korshunov A, Kool M, Pfister S, Cho YJ, Zhao K, and Crabtree GR (2013). BAF complexes facilitate decatenation of DNA by topoisomerase IIalpha. Nature 497, 624–627. [PubMed: 23698369]

Filippakopoulos P, Qi J, Picaud S, Shen Y, Smith WB, Fedorov O, Morse EM, Keates T, Hickman TT, Felletar I, et al. (2010). Selective inhibition of BET bromodomains. Nature 468, 1067–1073. [PubMed: 20871596]

Franke A, McGovern DP, Barrett JC, Wang K, Radford-Smith GL, Ahmad T, Lees CW, Balschun T, Lee J, Roberts R, et al. (2010). Genome-wide meta-analysis increases to 71 the number of confirmed Crohn's disease susceptibility loci. Nat. Genet 42, 1118–1125. [PubMed: 21102463]

Fraschilla I, and Jeffrey KL (2020). The speckled protein (SP) family: immunity's chromatin readers. Trends Immunol 41, 572–585. [PubMed: 32386862]

Friedrich M, Pohin M, and Powrie F (2019). Cytokine networks in the pathophysiology of inflammatory bowel disease. Immunity 50, 992–1006. [PubMed: 30995511]

Fukata M, Michelsen KS, Eri R, Thomas LS, Hu B, Lukasek K, Nast CC, Lechago J, Xu R, Naiki Y, et al. (2005). Toll-like receptor-4 is required for intestinal response to epithelial injury and limiting bacterial translocation in a murine model of acute colitis. Am. J. Physiol. Gastrointest. Liver Physiol 288, G1055–G1065. [PubMed: 15826931]

Gibson TJ, Ramu C, Gemünd C, and Aasland R (1998). The APECED polyglandular autoimmune syndrome protein, AIRE-1, contains the SAND domain and is probably a transcription factor. Trends Biochem. Sci 23, 242–244. [PubMed: 9697411]

Graham DB, and Xavier RJ (2020). Pathway paradigms revealed from the genetics of inflammatory bowel disease. Nature 578, 527–539. [PubMed: 32103191]

Hamon S, Le Sommer C, Mereau A, Allo MR, and Hardy S (2004). Polypyrimidine tract-binding protein is involved in vivo in repression of a composite internal/3′ -terminal exon of the Xenopus alpha-tropomyosin Pre-mRNA. J. Biol. Chem 279, 22166–22175. [PubMed: 15010470]

Härtlova A, Erttmann SF, Raffi FA, Schmalz AM, Resch U, Anugula S, Lienenklaus S, Nilsson LM, Kröger A, Nilsson JA, et al. (2015). DNA damage primes the type I interferon system via the cytosolic DNA sensor STING to promote anti-microbial innate immunity. Immunity 42, 332–343. [PubMed: 25692705]

He X, Yu J, Wang M, Cheng Y, Han Y, Yang S, Shi G, Sun L, Fang Y, Gong ST, et al. (2017). Bap180/Baf180 is required to maintain homeostasis of intestinal innate immune response in Drosophila and mice. Nat. Microbiol 2, 17056. [PubMed: 28418397]

Ho JSY, Mok BW, Campisi L, Jordan T, Yildiz S, Parameswaran S, Wayman JA, Gaudreault NN, Meekins DA, Indran SV, et al. (2021). Top1 inhibition therapy protects against SARS-CoV-2-induced lethal inflammation. Cell 184, 2618–2632.e17. [PubMed: 33836156]

Horita N, Yamamoto M, Sato T, Tsukahara T, Nagakura H, Tashiro K, Shibata Y, Watanabe H, Nagai K, Inoue M, et al. (2015). Topotecan for relapsed small-cell lung cancer: systematic review and meta-analysis of 1347 patients. Sci. Rep 5, 15437. [PubMed: 26486755]

Hu S, Peng L, Kwak YT, Tekippe EM, Pasare C, Malter JS, Hooper LV, and Zaki MH (2015). The DNA sensor AIM2 maintains intestinal homeostasis via regulation of epithelial antimicrobial Host Defense. Cell Rep 13, 1922–1936. [PubMed: 26655906]

Huoh YS, Wu B, Park S, Yang D, Bansal K, Greenwald E, Wong WP, Mathis D, and Hur S (2020). Dual functions of Aire CARD multimerization in the transcriptional regulation of T cell tolerance. Nat. Commun 11, 1625. [PubMed: 32242017]

Husain A, Begum NA, Taniguchi T, Taniguchi H, Kobayashi M, and Honjo T (2016). Chromatin remodeller SMARCA4 recruits topoisomerase 1 and suppresses transcription-associated genomic instability. Nat. Commun 7, 10549. [PubMed: 26842758]

International Multiple Sclerosis Genetics Consortium (IMSGC), Beecham AH, Patsopoulos NA, Xifara DK, Davis MF, Kemppinen A, Cotsapas C, Shah TS, Spencer C, Booth D, et al. (2013). Analysis of immune-related loci identifies 48 new susceptibility variants for multiple sclerosis. Nat. Genet 45, 1353–1360. [PubMed: 24076602]

Ji DX, Witt KC, Kotov DI, Margolis SR, Louie A, Chevée V, Chen KJ, Gaidt MM, Dhaliwal HS, Lee AY, et al. (2021). Role of the transcriptional regulator SP140 in resistance to bacterial infections via repression of type I interferons. eLife 10.

Jostins L, Ripke S, Weersma RK, Duerr RH, McGovern DP, Hui KY, Lee JC, Schumm LP, Sharma Y, Anderson CA, et al. (2012). Host-microbe interactions have shaped the genetic architecture of inflammatory bowel disease. Nature 491, 119–124. [PubMed: 23128233]

Ju BG, Lunyak VV, Perissi V, Garcia-Bassets I, Rose DW, Glass CK, and Rosenfeld MG (2006). A topoisomerase IIbeta-mediated dsDNA break required for regulated transcription. Science 312, 1798–1802. [PubMed: 16794079]

Karaky M, Fedetz M, Potenciano V, Andrés-León E, Codina AE, Barrionuevo C, Alcina A, and Matesanz F (2018). SP140 regulates the expression of immune-related genes associated with multiple sclerosis and other autoimmune diseases by NF-kappaB inhibition. Hum. Mol. Genet 27, 4012–4023. [PubMed: 30102396]

Kim JJ, Lee SY, Gong F, Battenhouse AM, Boutz DR, Bashyal A, Refvik ST, Chiang CM, Xhemalce B, Paull TT, et al. (2019). Systematic bromodomain protein screens identify homologous recombination and R-loop suppression pathways involved in genome integrity. Genes Dev 33, 1751–1774. [PubMed: 31753913]

Kobayashi M, Aida M, Nagaoka H, Begum NA, Kitawaki Y, Nakata M, Stanlie A, Doi T, Kato L, Okazaki IM, et al. (2009). AID-induced decrease in topoisomerase 1 induces DNA structural alteration and DNA cleavage for class switch recombination. Proc. Natl. Acad. Sci. USA 106, 22375–22380. [PubMed: 20018730]

Lallemand-Breitenbach V, and de Thé H (2010). PML nuclear bodies. Cold Spring Harb. Perspect. Biol 2, a000661. [PubMed: 20452955]

Lassen KG, Kuballa P, Conway KL, Patel KK, Becker CE, Peloquin JM, Villablanca EJ, Norman JM, Liu TC, Heath RJ, et al. (2014). Atg16L1 T300A variant decreases selective autophagy resulting in altered cytokine signaling and decreased antibacterial defense. Proc. Natl. Acad. Sci. USA 111, 7741–7746. [PubMed: 24821797]

Li H, and Durbin R (2009). Fast and accurate short read alignment with Burrows-Wheeler transform. Bioinformatics 25, 1754–1760. [PubMed: 19451168]

Loehrer PJ Sr.. (1991). Etoposide therapy for testicular cancer. Cancer 67, 220–224. [PubMed: 1984823]

Matesanz F, Potenciano V, Fedetz M, Ramos-Mozo P, Abad-Grau M, Karaky M, Barrionuevo C, Izquierdo G, Ruiz-Peña JL, García-Sánchez MI, et al. (2015). A functional variant that affects exon-skipping and protein expression of SP140 as genetic mechanism predisposing to multiple sclerosis. Hum. Mol. Genet 24, 5619–5627. [PubMed: 26152201]

Mathis D, and Benoist C (2009). Aire. Annu. Rev. Immunol 27, 287–312. [PubMed: 19302042]

McCarthy DJ, Chen Y, and Smyth GK (2012). Differential expression analysis of multifactor RNA-Seq experiments with respect to biological variation. Nucleic Acids Res 40, 4288–4297. [PubMed: 22287627]

Mehta S, Cronkite DA, Basavappa M, Saunders TL, Adiliaghdam F, Amatullah H, Morrison SA, Pagan JD, Anthony RM, Tonnerre P, et al. (2017). Maintenance of macrophage transcriptional programs and intestinal homeostasis by epigenetic reader SP140. Sci. Immunol 2, eaag3160. [PubMed: 28783698]

Mellacheruvu D, Wright Z, Couzens AL, Lambert JP, St-Denis NA, Li T, Miteva YV, Hauri S, Sardiu ME, Low TY, et al. (2013). The CRAPome: a contaminant repository for affinity purification-mass spectrometry data. Nat. Methods 10, 730–736. [PubMed: 23921808]

Miller EL, Hargreaves DC, Kadoch C, Chang CY, Calarco JP, Hodges C, Buenrostro JD, Cui K, Greenleaf WJ, Zhao K, et al. (2017). TOP2 synergizes with BAF chromatin remodeling for both resolution and formation of facultative heterochromatin. Nat. Struct. Mol. Biol 24, 344–352. [PubMed: 28250416]

Nicodeme E, Jeffrey KL, Schaefer U, Beinke S, Dewell S, Chung CW, Chandwani R, Marazzi I, Wilson P, Coste H, et al. (2010). Suppression of inflammation by a synthetic histone mimic. Nature 468, 1119–1123. [PubMed: 21068722]

Pan H, Yan BS, Rojas M, Shebzukhov YV, Zhou H, Kobzik L, Higgins DE, Daly MJ, Bloom BR, and Kramnik I (2005). Ipr1 gene mediates innate immunity to tuberculosis. Nature 434, 767–772. [PubMed: 15815631]

Peloquin JM, Goel G, Villablanca EJ, and Xavier RJ (2016). Mechanisms of pediatric inflammatory bowel disease. Annu. Rev. Immunol 34, 31–64. [PubMed: 27168239]

Pommier Y, Sun Y, Huang SN, and Nitiss JL (2016). Roles of eukaryotic topoisomerases in transcription, replication and genomic stability. Nat. Rev. Mol. Cell Biol 17, 703–721. [PubMed: 27649880]

Puc J, Aggarwal AK, and Rosenfeld MG (2017). Physiological functions of programmed DNA breaks in signal-induced transcription. Nat. Rev. Mol. Cell Biol 18, 471–476.

Rakoff-Nahoum S, Paglino J, Eslami-Varzaneh F, Edberg S, and Medzhitov R (2004). Recognition of commensal microflora by toll-like receptors is required for intestinal homeostasis. Cell 118, 229–241. [PubMed: 15260992]

Ramanan D, Tang MS, Bowcutt R, Loke P, and Cadwell K (2014). Bacterial sensor Nod2 prevents inflammation of the small intestine by restricting the expansion of the commensal Bacteroides vulgatus. Immunity 41, 311–324. [PubMed: 25088769]

Ramírez F, Dündar F, Diehl S, Grüning BA, and Manke T (2014). deep-Tools: a flexible platform for exploring deep-sequencing data. Nucleic Acids Res 42, W187–W191. [PubMed: 24799436]

Ren J, Gao X, Jin C, Zhu M, Wang X, Shaw A, Wen L, Yao X, and Xue Y (2009). Systematic study of protein SUMOylation: development of a site-specific predictor of SUMOsp 2.0. Proteomics 9, 3409–3412. [PubMed: 29658196]

Rialdi A, Campisi L, Zhao N, Lagda AC, Pietzsch C, Ho JSY, Martinez-Gil L, Fenouil R, Chen X, Edwards M, et al. (2016). Topoisomerase 1 inhibition suppresses inflammatory genes and protects from death by inflammation. Science 352, aad7993. [PubMed: 27127234]

Ross-Innes CS, Stark R, Teschendorff AE, Holmes KA, Ali HR, Dunning MJ, Brown GD, Gojis O, Ellis IO, Green AR, et al. (2012). Differential oestrogen receptor binding is associated with clinical outcome in breast cancer. Nature 481, 389–393. [PubMed: 22217937]

Sabari BR, Dall'Agnese A, Boija A, Klein IA, Coffey EL, Shrinivas K, Abraham BJ, Hannett NM, Zamudio AV, Manteiga JC, et al. (2018). Coactivator condensation at super-enhancers links phase separation and gene control. Science 361, eaar3958. [PubMed: 29930091]

Sauna ZE, and Kimchi-Sarfaty C (2011). Understanding the contribution of synonymous mutations to human disease. Nat. Rev. Genet 12, 683–691. [PubMed: 21878961]

Schneider CA, Rasband WS, and Eliceiri KW (2012). NIH Image to ImageJ: 25 years of image analysis. Nat. Methods 9, 671–675. [PubMed: 22930834]

Sillé FC, Thomas R, Smith MT, Conde L, and Skibola CF (2012). Post-GWAS functional characterization of susceptibility variants for chronic lymphocytic leukemia. PLoS One 7, e29632. [PubMed: 22235315]

Smale ST, Tarakhovsky A, and Natoli G (2014). Chromatin contributions to the regulation of innate immunity. Annu. Rev. Immunol 32, 489–511. [PubMed: 24555473]

Soshnev AA, Josefowicz SZ, and Allis CD (2016). Greater than the sum of parts: complexity of the dynamic epigenome. Mol. Cell 62, 681–694. [PubMed: 27259201]

Szklarczyk D, Gable AL, Lyon D, Junge A, Wyder S, Huerta-Cepas J, Simonovic M, Doncheva NT, Morris JH, Bork P, et al. (2019). STRING v11: protein-protein association networks with increased coverage, supporting functional discovery in genome-wide experimental datasets. Nucleic Acids Res 47, D607–D613. [PubMed: 30476243]

van Galen P, Viny AD, Ram O, Ryan RJ, Cotton MJ, Donohue L, Sievers C, Drier Y, Liau BB, Gillespie SM, et al. (2016). A multiplexed system for quantitative comparisons of chromatin landscapes. Mol. Cell 61, 170–180. [PubMed: 26687680]

Vos SM, Tretter EM, Schmidt BH, and Berger JM (2011). All tangled up: how cells direct, manage and exploit topoisomerase function. Nat. Rev. Mol. Cell Biol 12, 827–841. [PubMed: 22108601]

Wan L, Chong S, Xuan F, Liang A, Cui X, Gates L, Carroll TS, Li Y, Feng L, Chen G, et al. (2020). Impaired cell fate through gain-of-functin mutations in a chromatin reader. Nature 577, 121–126. [PubMed: 31853060]

Wen H, Li Y, Xi Y, Jiang S, Stratton S, Peng D, Tanaka K, Ren Y, Xia Z, Wu J, et al. (2014). ZMYND11 links histone H3.3K36me3 to transcription elongation and tumour suppression. Nature 508, 263–268. [PubMed: 24590075]

Wu SE, Hashimoto-Hill S, Woo V, Eshleman EM, Whitt J, Engleman L, Karns R, Denson LA, Haslam DB, and Alenghat T (2020). Microbiota-derived metabolite promotes HDAC3 activity in the gut. Nature 586, 108–112. [PubMed: 32731255]

Xue Y, Zhou Y, Wu T, Zhu T, Ji X, Kwon YS, Zhang C, Yeo G, Black DL, Sun H, et al. (2009). Genome-wide analysis of PTB-RNA interactions reveals a strategy used by the general splicing repressor to modulate exon inclusion or skipping. Mol. Cell 36, 996–1006. [PubMed: 20064465]

Yates A, Akanni W, Amode MR, Barrell D, Billis K, Carvalho-Silva D, Cummins C, Clapham P, Fitzgerald S, Gil L, et al. (2016). Ensembl 2016. Nucleic Acids Res 44, D710–D716. [PubMed: 26687719]

Zhao Q, Xie Y, Zheng Y, Jiang S, Liu W, Mu W, Liu Z, Zhao Y, Xue Y, and Ren J (2014). GPS-SUMO: a tool for the prediction of SUMOylation sites and SUMO-interaction motifs. Nucleic Acids Res 42, W325–W330. [PubMed: 24880689]

Zucchelli C, Tamburri S, Filosa G, Ghitti M, Quilici G, Bachi A, and Musco G (2019). Sp140 is a multi-SUMO-1 target and its PHD finger promotes SUMOylation of the adjacent bromodomain. Biochim. Biophys. Acta Gen. Subj 1863, 456–465. [PubMed: 30465816]

Highlights

- Mutations within immune epigenetic reader SP140 associate with Crohn's disease (CD)
- Proteomics-revealed SP140 suppresses topoisomerases (TOP1/2) at heterochromatin
- Mice and CD patients with loss of SP140 have uncontrolled macrophage TOP1/2
- TOP inhibitors rescued defective macrophage function and colitis due to SP140 loss

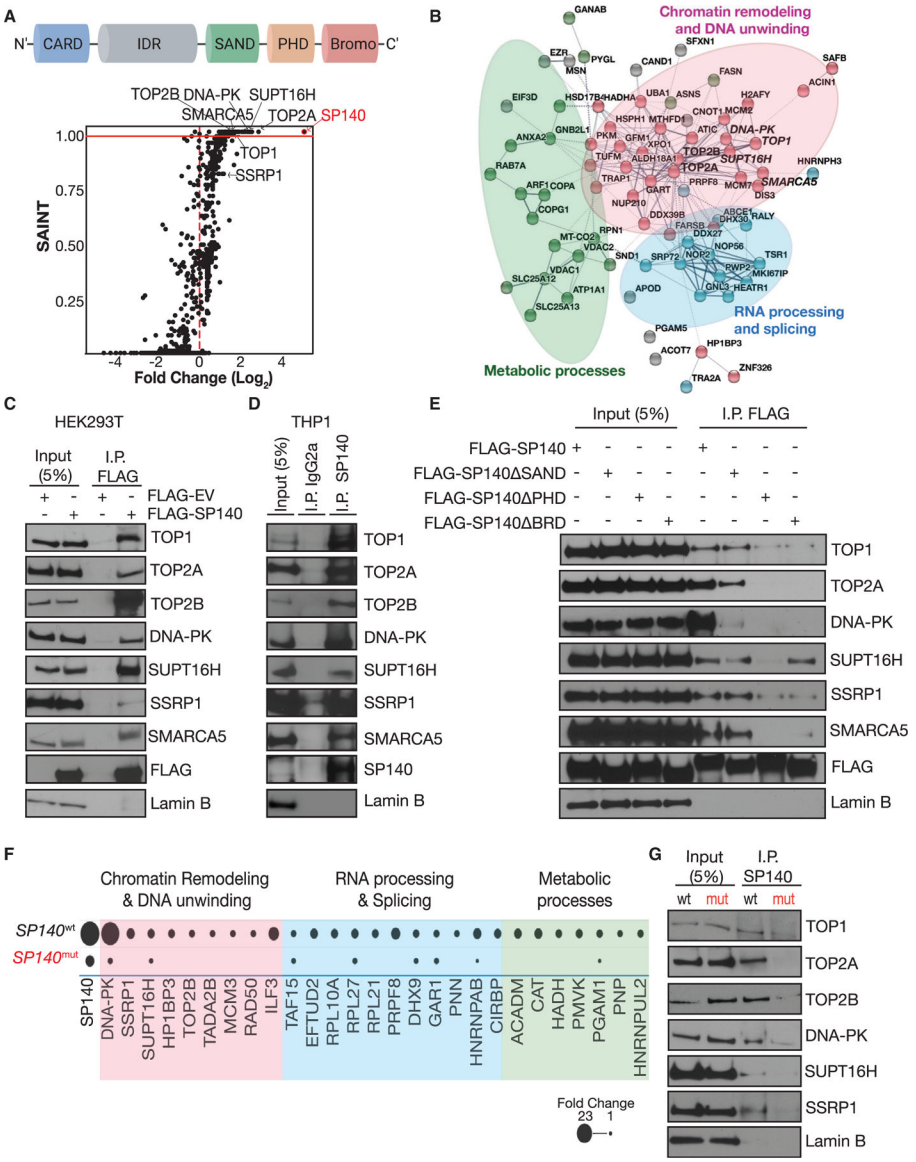

Figure 1. SP140 interactome includes DNA unwinding and chromatin remodeling proteins, including topoisomerases

(A) Schematic of SP140 protein domains. SP140-interacting proteins identified using mass spectrometry (MS) of HEK293T nuclear lysates overexpressing FLAG-SP140 plotted as $\log_2$-fold change (over FLAG empty vector control) versus significance analysis of interactome (SAINT) values. SAINT score ε 0.99 and FC > 2 is indicated above the red line. Data are generated from n = 2.

(B) Visual representation of SP140 interacting proteins (with SAINT score ε 0.99 and FC > 2) using k-means clustering on STRING database (https://string-db.org/).

(C) Immunoprecipitation (IP) of FLAG-EV and FLAG-SP140 and immunoblot for endogenous topoisomerase I (TOP1), topoisomerase II alpha (TOP2A) and beta (TOP2B), DNA-dependent protein kinase (DNA-PK) facilitates chromatin transaction (FACT) complex subunit SPT16 (SUPT16H), FACT complex subunit SSRP1 (SSRP1), and SWI/

SNF-related matrix-associated actin-dependent regulator of chromatin subfamily A member 5 (SMARCA5) in HEK293T nuclear lysates. Lamin B is loading control.

(D) IP of endogenous SP140 and immunoblot for indicated endogenous proteins in human THP1 monocyte nuclear lysates.

(E) IP of FLAG-SP140 or FLAG-SP140 mutants lacking reader modules SAND (SP140ΔSAND), plant homeobox domain (PHD, SP140ΔPHD), or bromodomain (SP140ΔBRD) and immunoblot for indicated endogenous proteins in HEK293T nuclear lysates.

(F) Mass spectrometry identification of SP140 interactors in patient-derived lymphoblastoid cell lines (LBL) with wild-type SP140 ($SP140^{wt}$) and SP140 Crohn's disease (CD)-risk SP140 mutations ($SP140^{mut}$). Data are fold change of endogenous SP140 IP mass spectrometry (MS) peptide hits over IgG IP control. All proteins identified are in Figure S6.

(G) IP of endogenous SP140 and immunoblot for indicated proteins in LBL nuclear lysates with indicated SP140 genotypes.

(C–E) are representative of 3 experiments, (F) is mean of two biological replicates of each SP140 genotype, and (G) is representative of 2 experiments.

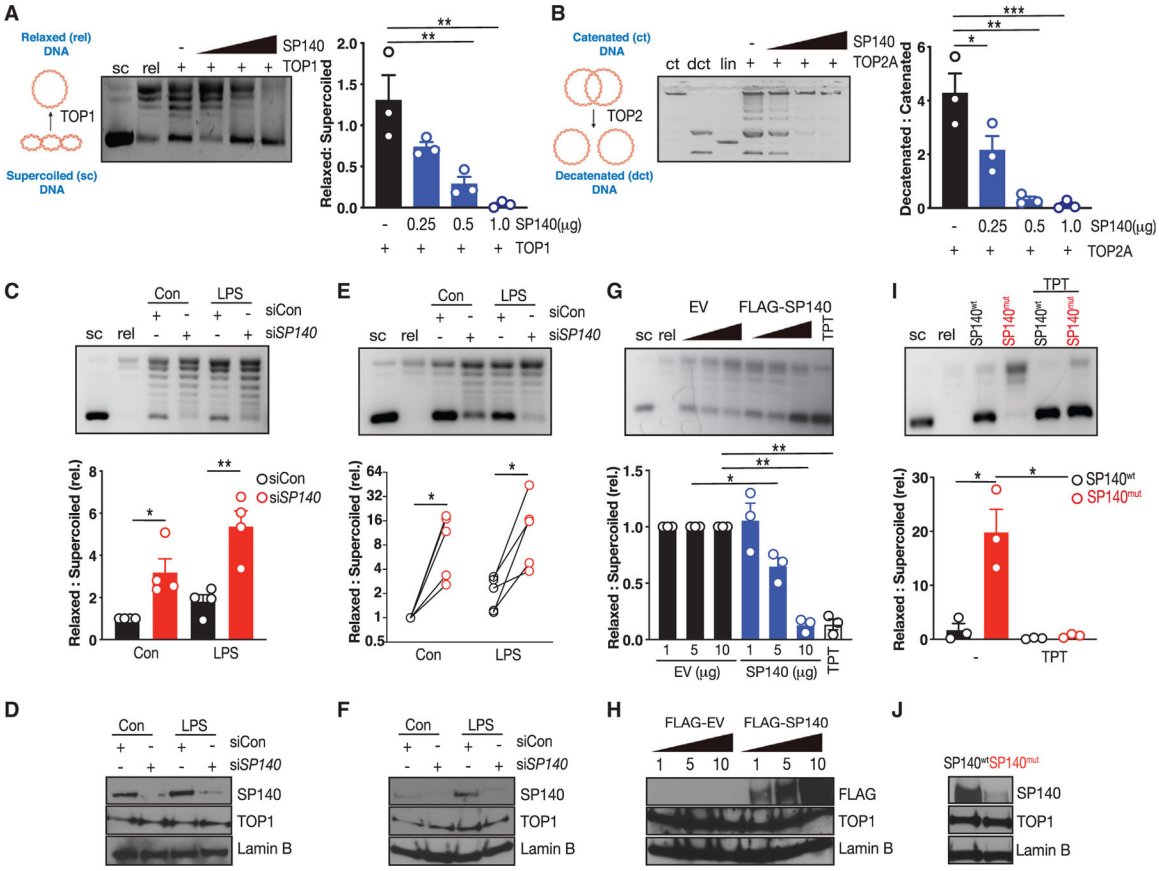

Figure 2. SP140 is a suppressor of topoisomerases TOP1 and TOP2

(A) Left, schematic of topoisomerase 1 (TOP1) activity assay using migration and quantification of supercoiled (sc) and relaxed (rel) DNA following incubation of TOP1 with supercoiled pHOT DNA. Right, representative gel image and quantification of recombinant TOP1 activity (10 activity units, ~120 ng) in the presence of indicated concentrations of recombinant full length SP140.

(B) Left, schematic of topoisomerase 2 (TOP2) activity assay using migration and quantification of catenated (ct) and decatenated (dct) DNA following incubation of TOP2A with catenated DNA. Right, representative image and quantification of recombinant TOP2A (8 activity units, ~110 ng) activity in the presence of indicated concentrations of recombinant full length SP140. Linear DNA (lin) serves as an assay control.

(C) Representative gel image and quantification of TOP1 activity assay in nuclear lysates from control (black bars) or siRNA-mediated SP140 knockdown (KD, red bars) naive or LPS (100 ng/mL, 4 h)-stimulated THP1 monocytes.

(D) Immunoblot of SP140 and TOP1 in control or SP140 siRNA-mediated knockdown THP1 monocytes.

(E) Representative gel image and quantification of TOP1 activity assay in nuclear lysates from control (black circles) or SP140 KD (red circles) naive or LPS (100 ng/mL, 4 h)-stimulated primary human peripheral blood-derived macrophages. Connecting lines indicate individual healthy blood donors.

(F) Immunoblot of SP140 and TOP1 in control or SP140 siRNA-mediated knockdown primary human macrophage nuclear lysates.
(G) Representative gel image and quantification of TOP1 activity assay in nuclear lysates from HEK293T cells transfected with indicated concentrations of FLAG empty vector (EV, black bars) or FLAG-SP140 (blue bars) or treated with Topotecan (TPT, 100 μM).
(H) Immunoblot of FLAG and TOP1 in HEK293T nuclear lysates transfected with indicated concentrations of FLAG empty vector (EV) and FLAG-SP140 (μg).
(I) Representative gel image and quantification of TOP1 activity assay in lymphoblastoid cell lines (LBL) bearing wild-type SP140 ($SP140^{wt}$) or CD-risk SP140 genetic variants ($SP140^{mut}$) in the presence or absence of TPT (100 μM).
(J) Immunoblot of SP140 and TOP1 in lymphoblastoid cell lines (LBL) with wild-type SP140 ($SP140^{wt}$) or Crohn's disease (CD)-risk SP140 mutations ($SP140^{mut}$). Lamin B is loading control.
Errors bars are SEM. *$p < 0.05$, **$p < 0.01$, ***$p < 0.001$; two-tailed, unpaired t test.

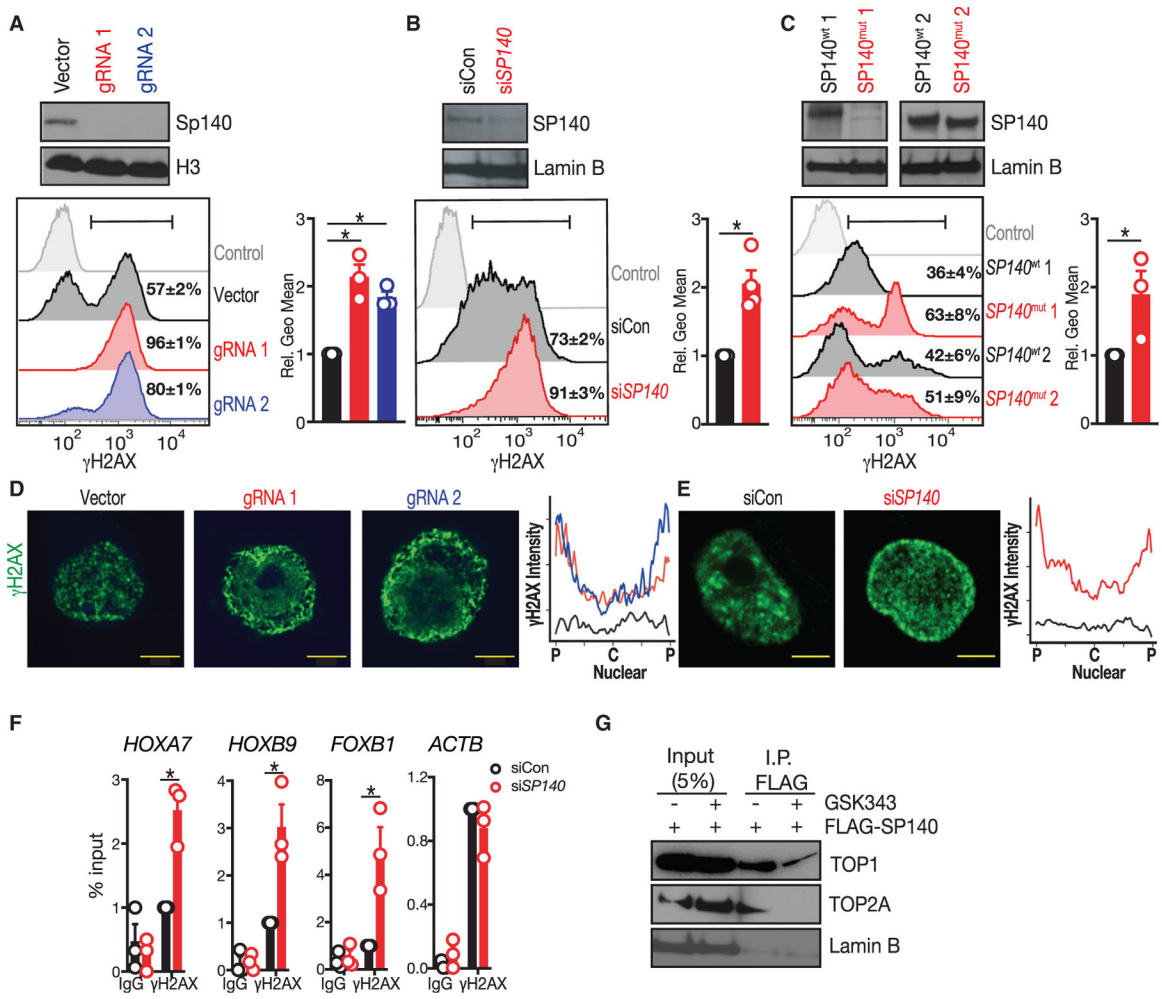

Figure 3. Loss-of-function SP140 or SP140 deletion increases DNA double-strand breaks on heterochromatin

(A–C) Quantification of DNA double-stranded breaks as assessed by γH2AX (phospho S139) in (A), vector control or Sp140 CRISPR-deleted Sp140 Cas9 transgenic immortalized mouse bone marrow macrophages (BMDMs) using two separate guide (g)RNAs (B), control, or *SP140* siRNA-mediated knockdown THP1 cells or (C), race- and sex-matched lymphoblastoid B cell lines (LBLs) bearing wild-type SP140 ($SP140^{wt}$) or SP140 disease-risk mutations ($SP140^{mut}$) by flow cytometry. Mean and SEM. γH2AX% positive cells are indicated in histogram gates, adjacent graphs are (Γ)H2AX geometric mean relative to control.

(D and E) (D) Cell localization of γH2AX in vector control or Sp140 CRISPR-deleted Sp140 Cas9 transgenic immortalized mouse bone marrow macrophages (BMDMs) or (E), control or *SP140* siRNA-mediated knockdown THP1 cells as assessed by confocal microscopy. Scale bars, 5 μm. Line plots are the average quantification of γH2AX fluorescence intensity across the nuclear diameter (p = periphery, c = center) of 25 cells using ImageJ.

(F) γH2AX chromatin immunoprecipitation quantitative PCR (ChIP qPCR) of *HOXA7*, *HOXB9*, *FOXB1*, or *ACTB* in control (black) and SP140 knockdown (red) primary human

macrophages, represented as % of input and normalized to siCon of each blood donor. IgG ChIP served as a negative control.

(G) Co-immunoprecipitation of FLAG SP140 and endogenous TOP1 and TOP2A in HEK293T cells treated with GSK343 (2.5 μM).

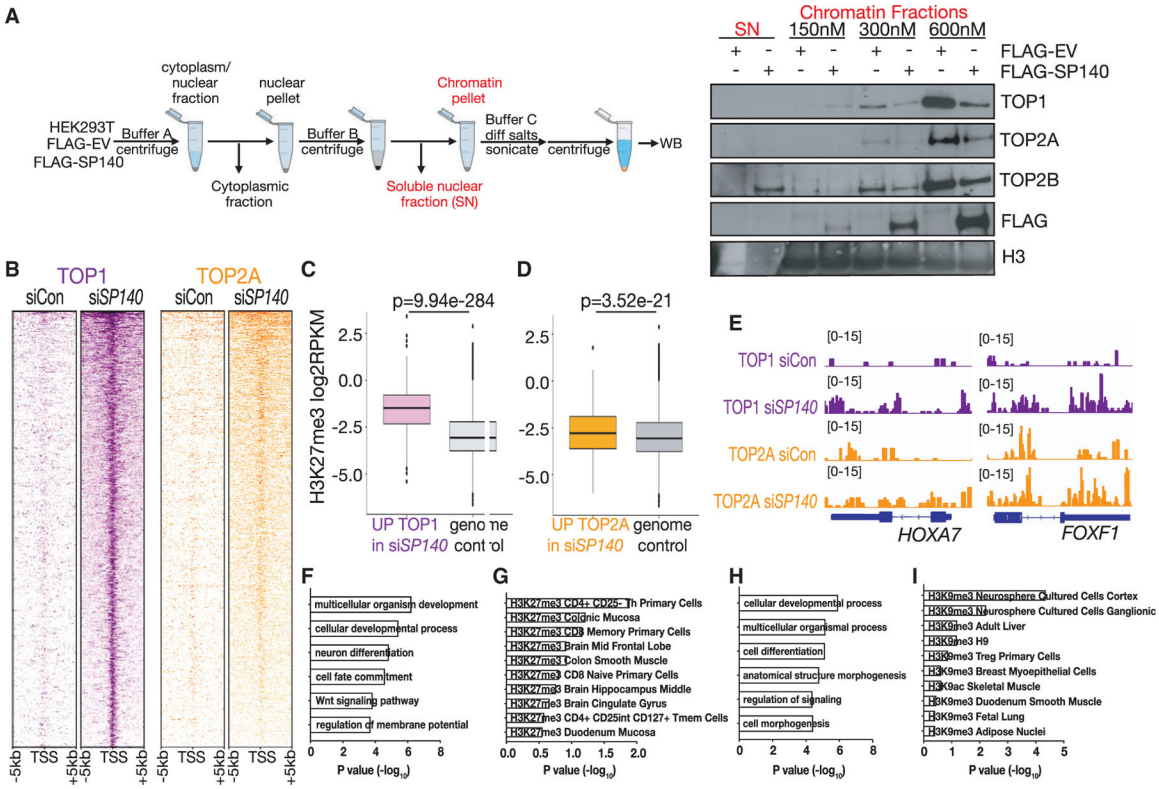

Figure 4. SP140 shields topoisomerases 1 and 2 from heterochromatin

(A) Left, schematic of chromatin fractionation protocol. Right, immunoblot of soluble nuclear (SN) fraction and chromatin fractions isolated from nuclei of FLAG EV, FLAG SP140 overexpressing HEK293T cells lysed with indicated concentrations of NaCl.

(B) Heatmaps of TOP1 (purple) or TOP2 (orange) CUT&Tag peaks in transcriptional start site (TSS) proximal regions (TSS ± 5 kb) in control or *SP140*-knockdown primary human macrophages rank-ordered by occupancy in control.

(C and D) (C) H3K27me3 density (log_2 scale), as determined by multiplexed indexed chromatin immunoprecipitation (MintChIP) at TSS-proximal regions (TSS ± 3 kb) of genes that significantly increased TOP1 (purple) or (D), TOP2 (orange) occupancy in SP140 knockdown human macrophages compared with genomic control (gray). RPKM, reads per kilobase, per million mapped reads.

(E) CUT&Tag genomic tracks of TOP1 (purple) and TOP2A (orange) densities at *HOXA7* and *FOXF1* in control and SP140 knockdown primary human macrophages.

(F and G) (F) Gene ontology biological processes or (G) epigenomics roadmap signature of loci that gained TOP1 occupancy in SP140 knockdown primary human macrophages (fold-change > 2, FDR < 0.01) as assessed by CUT&Tag.

(H and I) (H) Gene ontology biological processes or (I) epigenomics roadmap signature of genes that gained TOP2A occupancy in SP140 knockdown primary human macrophages (fold-change > 2, FDR < 0.01) as assessed by CUT&Tag. *p < 0.05. Data are mean of 3–4 biological replicates. Error bars are SEM. *p < 0.05; two-tailed, unpaired t test.

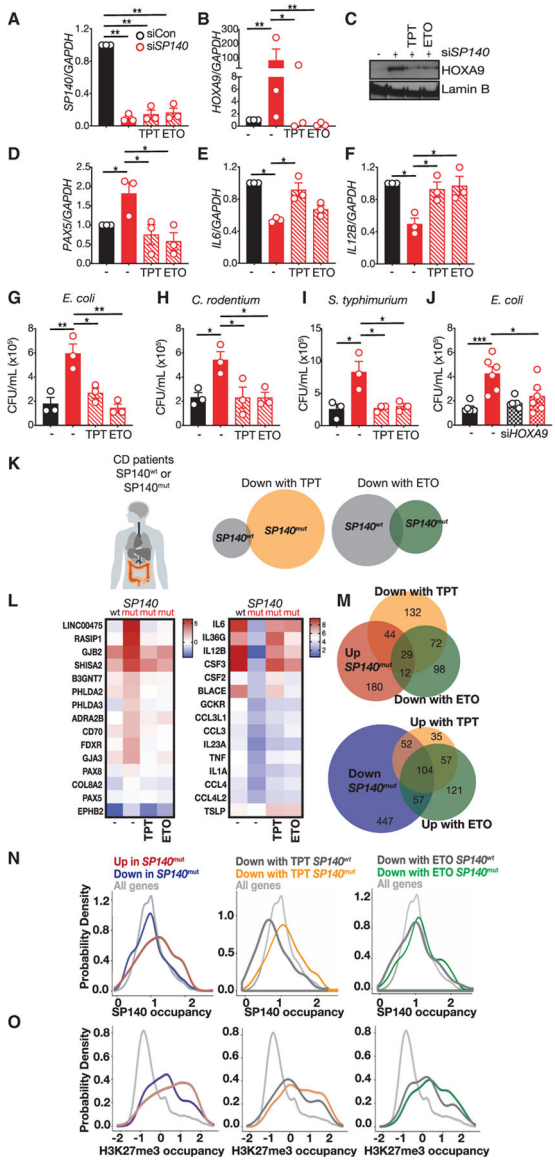

Figure 5. TOP inhibitors rescue defective innate immune transcriptional programs in SP140 loss-of-function Crohn's disease patients

(A–F) (A) Levels of *SP140*, (B and C) *HOXA9*, (D) *PAX5*, (E) *IL6*, and (F) *IL12B* in control (black) and SP140 knockdown (red) primary human macrophages from healthy donors in the absence or presence of topoisomerase I inhibitor, Topotecan (TPT, 100 nM) or topoisomerase II inhibitor, Etoposide (ETO, 25 μM) as assessed by quantitative PCR or western blot. Data are normalized to DMSO siControl of each human blood donor. Lamin B is loading control. Data are mean of three biological replicates. Error bars are SEM. *p < 0.05, **p < 0.01; one-way ANOVA with Tukey's multiple comparisons test.

(G–I) (G) Gentamicin protection assay on control or SP140 siRNA-mediated knockdown primary human macrophages treated with TPT (100 nM) or ETO (25 μM) and spin-infected with Crohn's disease-associated *Escherichia coli* (*E. coli*, 10 CFU/cell), (H) *Citrobacter rodentium* (*C. rodentium*, 10 CFU/cell), or (I) *Salmonella enterica* serovar typhimurium (*S. typhimurium*, 10 CFU/cell).

(J) Gentamicin protection assay of control, *SP140* siRNA-mediated knockdown or SP140/HOXA9 double knockdown primary human macrophages infected with *E. coli* (*E. coli*, 10 CFU/cell). Each dot is the average of a technical triplicate per individual blood donor. Error bars are SEM. *$p < 0.05$, **$p < 0.01$; one-way ANOVA with Tukey's multiple comparisons test.

(K) Fresh peripheral blood mononuclear cells (PBMCs) were obtained from CD patients carrying wild-type SP140 ($SP140^{wt}$) or were homozygous for SP140 disease-associated mutations ($SP140^{mut}$). Venn diagram of downregulated genes (fold change, FC > 2) in CD patient $SP140^{wt}$ (gray) or $SP140^{mut}$ PBMCs by Topotecan (TPT, 100 nM, orange) or Etoposide (ETO, 25 μM, green) as determined by RNA-seq.

(L) Heatmap of expression changes (log_2 FC) among top 15 differentially expressed genes in $SP140^{mut}$ compared with $SP140^{wt}$ that were rescued with TPT or ETO in LPS (100 ng/mL, 4 h)-stimulated PBMCs.

(M) Venn diagram of up or downregulated genes ($log_2FC > 1$) in CD patient $SP140^{mut}$ PBMCs compared with $SP140^{wt}$ which were reversed by $log_2FC > 1$ with TPT or ETO.

(N and O) (N) Distribution (probability density function) of levels of SP140 enrichment (human macrophage ChIP-seq[12]) or (O) H3K27me3 (average of ENCODE data ENCSR553XBX, ENCSR866UQO, and ENCSR390SFH) in the TSS-proximal region for all genes (gray) compared with genes that were upregulated (red) or downregulated (blue) in $SP140^{mut}$ PBMCs compared with $SP140^{wt}$ PBMCs or TPT-(orange) or ETO-downregulated (green) genes in $SP140^{wt}$ or $SP140^{mut}$ PBMCs.

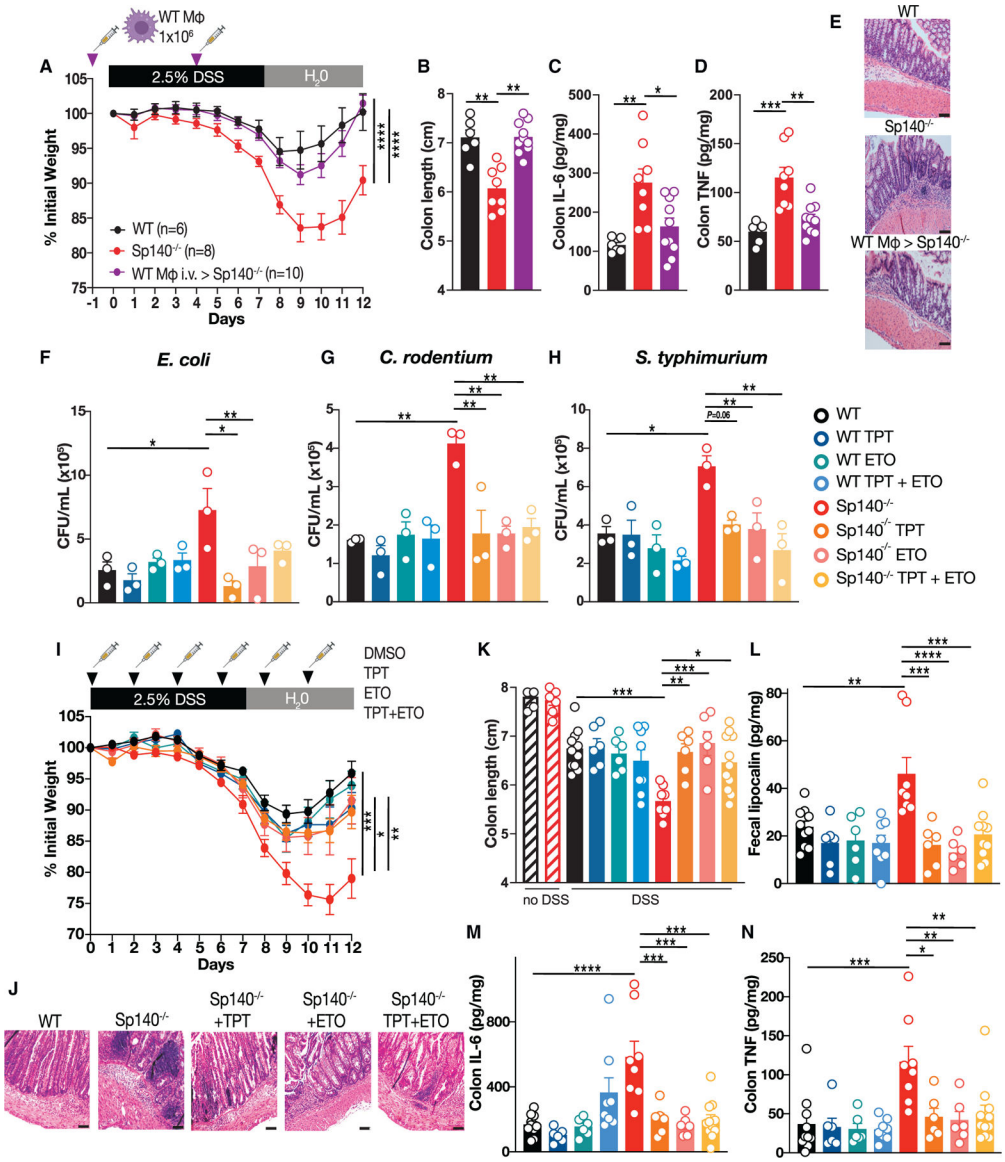

Figure 6. Precision rescue of DSS colitis in Sp140 knockout mice with TOP inhibition

(A) Daily body weight measurements after 2.5% DSS administration in drinking water for 7 days followed by water administration to wild type (WT), Sp140$^{-/-}$, or Sp140$^{-/-}$ mice administered WT bone marrow-derived macrophages (Mϕ, 1 3 10^6, i.v. 1 day prior and 4 days after DSS commencement).

(B) Colon length at baseline or day 12 of DSS.

(C and D) (C) Interleukin (IL)-6 or (D) TNF levels in day 12 colonic explant supernatants cultured for 24 h.

(E) Representative hematoxylin and eosin (H&E) staining of distal colon sections of WT, Sp140$^{-/-}$, and WT Mϕ > Sp140$^{-/-}$ mice at day 12. Scale bars, 100 μm.

(F–H) (F) Gentamicin protection assay using wild type (WT) or SP140 CRISPR-deleted (Sp140$^{-/-}$) bone-marrow-derived macrophages treated with TPT (100 nM) or ETO (25 μM) and spin-infected with Crohn's disease-associated *Escherichia coli* (*E. coli*, 10 CFU/cell),

(G) *Citrobacter rodentium* (*C. rodentium*, 10 CFU/cell), or (H) *Salmonella enterica* serovar typhimurium (*S. typhimurium*, 10 CFU/cell). Each dot is the average of a technical triplicate per individual mouse. Error bars are SEM. *p < 0.05, **p < 0.01; one-way ANOVA with Tukey's multiple comparisons test.

(I) Daily body weight measurements in WT and $Sp140^{-/-}$ mice after 2.5% DSS administration in drinking water for 7 days followed by water and intraperitoneal (i.p.) administration of DMSO control, TPT (1 mg/kg), ETO (1 mg/kg), or TPT+ETO (1 mg/kg + 1 mg/kg) every other day as indicated with black arrow.

(J) Representative hematoxylin and eosin (H&E) staining of distal colon sections of WT and $Sp140^{-/-}$ with and without inhibitors in mice at day 12. Scale bars, 100 μm.

(K) Colon length at baseline or day 12 of DSS.

(L) Fecal lipocalin-2 (Lcn-2) content at day 9 of DSS.

(M and N) (M) Interleukin(IL)-6 or (N) TNF levels in day 12 colonic explant supernatants cultured for 24 h. *p < 0.05, **p < 0.01, ***p < 0.001, ****p < 0.0001; one-way ANOVA with Tukey's multiple comparisons test.

KEY RESOURCES TABLE

REAGENT or RESOURCE	SOURCE	IDENTIFIER
Antibodies		
FLAG-M2	Sigma	F1804
Topoisomerase 1	Abcam	ab85038
Topoisomerase 2a	Abcam	ab52934
Topoisomerase 2b	R&D	MAB6348
DNA-PK	Cell Signaling	12311
SUPT16H	Abcam	ab108960
SSRP1	Abcam	ab26212
SMARCA5	Abcam	ab72499
HA	Abcam	ab9110
HOXA9	Abcam	ab83480
SP140	Sigma	HPA006162
Lamin B	Cell Signaling	12586S
γH2AX	abcam	ab2893
Chk2	Millipore Obtained from laboratory of Raul Mostoslavsky	05-649
phospho-Chk2	Cell Signaling Obtained from laboratory of Raul Mostoslavsky	2661
AlexaFluor 488	Life technologies	A11008
Bacterial and virus strains		
Stbl3 bacteria	Invitrogen	C7373-03
Biological samples		
Healthy human peripheral blood derived macrophages	MGH Blood Components Lab	N/A
Crohn’s disease peripheral blood mononuclear cells	PRISM Cohort, MGH	N/A
Chemicals, peptides, and recombinant proteins		
DMEM media	Life technologies	11995-073
RPMI media	Life technologies	11875-093
OptiMEM media	Life technologies	31485-070
X Vivo 10 media	Lonza	BEBP0Z-0550
Dextran Sodium Sulfate	MP Biomedicals	160110
Hyclone fetal bovine serum	GE Healthcare	S#30396.03
Penicillin-Streptomycin	Gibco	P4333
Ficoll-Paque Plus	GE Healthcare	17-1440-02
Lipofectamine 2000	Life Technologies	11668027
RNAiMAX	Life Technologies	13778075
HiPerfect Transfection Reagent	Qiagen	1029975
Mnase	NEB	M0247S

REAGENT or RESOURCE	SOURCE	IDENTIFIER
Recombinant Human Top1	Topogen	TG2005H-RC1
Recombinant Human Top2A	Topogen	TG2000H-1
CUTANA pAG-Tn5	Epicypher	15-1017
CUTANA High Fidelity 2x PCR Master Mix	Epicypher	15-1018
CUTANA Concanavalin A beads	Epicypher	21-1401
Dynabeads MyONE Silane beads	Thermofisher	37002D
REAGENT or RESOURCE	SOURCE	IDENTIFIER
AMPure SPRI beads	Beckman Coulter	A63880
Dynabeads Protein G	Thermofisher	10004D
Topotecan	Sigma	1672257
Etoposide	Sigma	E1383
LPS 0111:B4	Sigma	14391
Human M-CSF	Peprotech	300-25
Human IFN-g	Peprotech	300-02
16% Formaldehyde	Thermofisher	28908
ProLong Diamond Antifade Mountant	Thermo Fisher Scientific	P36970
Alexa Fluor® 488 annexin V/Dead Cell Apoptosis Kit	Thermofisher	V13241
Ethidium Bromide	Promega	H5041
Critical commercial assays		
Topoisomerase I Activity Assay Kit	Topogen	TG1015-1
Topoisomerase II Activity Assay Kit	Topogen	TG1001-1
truChIP Shearing Kit	Covaris	520154
RNease mini kit	Qiagen	74104
NEBnext Ultra II RNA library prep kit	NEB	E7770S
NEB HiScribe T7 kit	NEB	E2050S
Mouse IL-6 ELISA kit	R&D	DY406
Mouse TNF ELISA kit	R&D	DY410
Mouse Lipocalin-2 ELISA kit	R&D	DY1857
Monarch DNA PCR Clean Kit	NEB	T1030S
Deposited data		
PBMC RNAseq data	This paper	GEO: GSE161031
TOP1 and TOP2A Human macrophage CUT&Tag data	This paper	GEO: GSE174466
H327me3 Human macrophage MINT ChIP data	This paper	GEO: GSE178632
Experimental models: Cell lines		
Human: HEK293T cells	Laboratory of Terry Means	N/A
Human: THP1	Laboratory of Hans-Christian Reinecker	N/A
Mouse: Cas9 immortalized macrophages	Laboratory of Katherine A Fitzgerald	N/A

REAGENT or RESOURCE	SOURCE	IDENTIFIER
Experimental models: Organisms/strains		
Mouse: C57BL6/J	The Jackson Laboratory	JAX: 000664
Mouse: SP140 Knockout (on C57BL6/J background)	Laboratory of Russell Vance	(Ji et al., 2021)
Oligonucleotides		
ON-TARGETplus Non-targeting Control Pool UGGUUUACAUGUCGACUAA, UGGUUUACAUGUUGUGUGA, UGGUUUACAUGUUUUCUGA, UGGUUUACAUGUUUUCCUA	Dharmacon/Horizons Discovery	D-001810-10-05
ON-TARGETplus Human SP140 siRNA – SMART pool CCGAGCAGAUGUAUGA ACA, CAAGAGUGAUGUAUUGUGU, GAACGUAGAGGGUCAGAAC, GGAUUAACCUGAUGGCCUA	Dharmacon/Horizons Discovery	L-016508-00-0005
siGENOME Non-Targeting siRNA Pool#1 UAGCGACUAAACACAUCAA, UAAGGCUAUGAAGAGAUAC, AUGUAUUGGCCUGUAUUAG, AUGAACGUGAAUUGCUCAA	Dharmacon/Horizons Discovery	D-001206-13-05
siGENOME SMARTpool Human TOP1 GAAAGGAAAUGACUAAUGA, GAAGAAG GCUGUUCAGAGA, GGAAGUAGCUACGU UCUUU, ACAUAAAGGUCCAGUAUUU	Dharmacon/Horizons Discovery	M-005278-00-0005
siGENOME SMARTpool Human TOP2A CAAACUACAUUGGCAUUUA, GAAAGAG UCCAUCAGAUUU, CGAAAGGAAUGGUU AACUA, AGUGACAGGUGGUCGAAAU	Dharmacon/Horizons Discovery	M-004239-02-005
siGENOME SMARTpool Human PRKDC GCAAAGAGGUGGCAGUUAA, GAGCAU CACUUGCCUUUAA, GAUGAGAAGUCC UUAGGUA, GCAGGACCGUGCAAGGUUA	Dharmacon/Horizons Discovery	M-005030-01-0005
Primer for Human qPCR SP140 F- TCTTTGACTGAGCACCGAGG R- ATTGCTGTCTCCACTTGCCA	IDT, (Mehta et al., 2017)	N/A
Primer for Human qPCR IL6 F- TCTCCACAAGCGCCTTCG R- CTCAGGGCTGAGATGCCG	IDT, (Mehta et al., 2017)	N/A
Primer for Human qPCR IL12B F- ACCAGAGCAGTGAGGTCTTA R- CTCCTTTGTGACAGGTGTACTG	IDT, this paper	N/A
Primer for Human qPCR HOXA7 F- TGAGGCCAATTTCCGCATCT R- CGTCAGGTAGCGGTTGAAGT	IDT, (Mehta et al., 2017)	N/A
Primer for Human qPCR GAPDH F- AGGGCTGCTTTTAACTCTGGT R- CCCCACTTGATTTTGGAGGGA	IDT, (Mehta et al., 2017)	N/A
Primer for Human qPCR HOXA9 F- ATGGCATTAAACCTGAACCG R- GTCTCCGCCGCTCTCTCATTC	IDT, (Mehta et al., 2017)	N/A
Primer for Human qPCR PAX5 F- GAGCGGGTGTGTGACAATGA R- GCACCGGCGACTCCTGAATAC	IDT, this paper	N/A
Primer for Human HOXA7 ChIP qPCR DNA F- GACGCCTACGGCAACT R- GCCTTTGGCGAGGTCACT	IDT, this paper	N/A
Primer for Human HOXB9 ChIP qPCR DNA F- ACCGCACTCCATATCGAGGAT R- GGTAGCTGGGGCTGAGGTTA	IDT, this paper	N/A
Primer for Human FOXB1 ChIP qPCR DNA F- TTCCTCATACCTTCACACGGC R- GCCAGCTCTGGTTTCTTTCAC	IDT, this paper	N/A
Primer for Human ACTB ChIP qPCR DNA F- TCGATATCCACGTGACATCCA R- GCAGCATTTTTTTACCCCCTC	IDT, this paper	N/A
Mouse guide RNA# 1 against Sp140 TGTTGGGGAACATATGACAC	Sigma	N/A
Mouse guide RNA#2 against Sp140 AAGGAAAAATTCAAACAAGG	Sigma	N/A
Recombinant DNA		
Plasmid: FLAG-Empty Vector (EV)	This paper	N/A
Plasmid: FLAG-SP140	This paper	N/A

REAGENT or RESOURCE	SOURCE	IDENTIFIER
Plasmid: HA-Aire	From Laboratory of Sun Hur	N/A
Plasmid: lentiGuide-puro	Addgene	52963
Plasmid: pVSVg	Addgene	8454
Plasmid: psPAX2	Addgene	12260
Software and algorithms		
STAR aligner	(Dobin et al., 2013)	N/A
bwa version 0.7.17	(Li et al., 2009)	N/A
Htseq	(Anders et al., 2015)	N/A
Ensembl Gene annotation	(Yates et al., 2016)	N/A
EdgeR package	(McCarthy et al., 2012)	N/A
Diffbind R package	(Ross-Innes et al., 2012)	N/A
DeepTools	(Ramirez et al., 2014)	N/A
FlowJo software	BD	http://flowjo.com
Graphpad Prism v9.1.2	Graphpad software	https://www.graphpad.com/
ImageJ	(Schneider et al., 2012)	https://imagej.nih.gov/ij/
Other		
iTaq Universal SYBR Green supermix	Bio Rad	1725124
iScript cDNA Synthesis Kit	Bio Rad	1708841